UCRL 8678

UNIVERSITY OF CALIFORNIA
Ernest O. Lawrence Radiation Laboratory

MECHANISMS OF THE (α,pn) REACTION

TWO-WEEK LOAN COPY

This is a Library Circulating Copy which may be borrowed for two weeks. For a personal retention copy, call Tech. Info. Division, Ext. 5545

DISCLAIMER

This document was prepared as an account of work sponsored by the United States Government. While this document is believed to contain correct information, neither the United States Government nor any agency thereof, nor the Regents of the University of California, nor any of their employees, makes any warranty, express or implied, or assumes any legal responsibility for the accuracy, completeness, or usefulness of any information, apparatus, product, or process disclosed, or represents that its use would not infringe privately owned rights. Reference herein to any specific commercial product, process, or service by its trade name, trademark, manufacturer, or otherwise, does not necessarily constitute or imply its endorsement, recommendation, or favoring by the United States Government or any agency thereof, or the Regents of the University of California. The views and opinions of authors expressed herein do not necessarily state or reflect those of the United States Government or any agency thereof or the Regents of the University of California.

UCRL-8678
Chemistry-General

UNIVERSITY OF CALIFORNIA

Lawrence Radiation Laboratory
Berkeley, California

Contract No. W-7405-eng-48

MECHANISMS OF THE (α,pn) REACTION

Robert Joseph Silva

(Thesis)

March 1959

Printed for the U. S. Atomic Energy Commission

Printed in USA. Price $2.00. Available from the
Office of Technical Services
U.S. Department of Commerce
Washington 25, D. C.

MECHANISMS OF THE (α,pn) REACTION

Contents

Abstract..... 4

I. Introduction..... 6

II. Experimental Procedures..... 11

Radiochemically Determined Cross Sections..... 11

A. Target Assemblies and Cyclotron Irradiations.. 11

B. Target Preparation..... 11

1. Nickel-60..... 11

2. Nickel-62..... 12

3. Selenium-80..... 12

4. Palladium-110..... 12

5. Lanthanum-139..... 13

C. Chemical Separations..... 13

1. Nickel-60 Bombardment..... 13

2. Nickel-62 Bombardment..... 14

3. Selenium Bombardments..... 14

4. Palladium Bombardments..... 14

5. Lanthanum Bombardments..... 15

D. Counting Instruments, Counting Technique, and Treatment of Data..... 15

1. Palladium Bombardment..... 15

2. Nickel-60 Bombardment..... 16

3. Nicke-62m Selenium, and Lanthanum Bombardments..... 17

E. Cross-Section Calculations..... 17

Scattering Chamber Investigations..... 18

A. Scattering Chamber..... 18

B. Targets..... 19

C. Detectors..... 19

1. Δ E Counter..... 19

2. E Counter..... 22

3. Foil Wheel..... 22

D. Electronic Particle Identifier..... 23
E. Pulse-Height Analyzer..... 24
F. Alignment of the Electronic Particle Identifier..... 24
G. Method of Operation..... 25
1. Energy Spectra..... 25
2. Particle Spectra..... 29
III. Results..... 30
A. Radiochemically Determined Cross Sections..... 30
B. Scattering-Chamber Studies..... 30
1. Introduction..... 30
2. Deuteron Energy Selection..... 35
3. Deuteron Cross Sections..... 36
4. Proton Energy Selection..... 39
5. Proton Cross Sections..... 48
6. Proton Spectra Contamination..... 57
IV. Discussion..... 59
A. Angular Distributions, Energy Spectra, and Cross Sections Expected from Statistical-Model and Optical-Model Interactions..... 59
B. Butler's Theory..... 62
C. Angular Distribution from $Be^9(\alpha,d)B^{11}$ and $Be^9(\alpha,p)B^{12}$ Reactions..... 64
D. Energy Spectra and Angular Distributions of Protons and Deuterons Involving Transitions to Many Levels..... 65
E. Discussion of Radiochemically Determined Cross Sections and Comparison With Scattering-Chamber Cross Sections..... 67
F. Conclusions..... 73
Acknowledgments..... 74
References..... 75

MECHANISMS OF THE (α,pn) REACTION

Robert Joseph Silva
Lawrence Radiation Laboratory and Department of Chemistry
University of California, Berkeley, California
March 1959

ABSTRACT

Radiochemically determined excitation functions have been measured for the (α,pn) nuclear reactions of Ni^{60}, Ni^{62}, Se^{80}, Pd^{110}, and La^{139} by using helium ions of 20 to 48 Mev. These data, combined with published and unpublished data of other workers, show the general trends in the (α,pn) reaction of elements ranging from Fe^{54} to Cf^{252}.

Energy spectra and angular distributions of deuterons and protons, produced in bombardments with helium ions of 40 and 48 Mev, have been obtained for Be^{9}, Al^{27}, Ni^{60}, Pd^{110}, Bi^{209}, and U^{238} by using scattering-chamber methods. Experimental limitations restricted the study to helium-ion bombarding energies greater than 40 Mev, and observed proton and deuteron energies of greater than about 15 Mev. The energy spectra and angular distributions are similar to those characteristic of the optical-model component of nuclear reactions; i.e., energy spectra that exhibit broad distributions with large contributions from particles of high energy, and angular distributions that show very strong forward peaking with little contribution from angles greater than 90°.

Total integrated cross sections for the (α,d) and (α,pn) reactions have been calculated from the energy spectra and angular distributions of the protons and deuterons. A simple mechanism, involving the prompt emission of a high-energy proton followed by neutron evaporation, was used to calculate the (α,pn) cross sections.

Most of the features of the radiochemically determined excitation functions can be explained by emission of high-energy deuterons and protons by direct-interaction processes. The (α,d)

and (α,pn) cross sections calculated from the scattering-chamber data can account for nearly all the radiochemically determined (α,pn) cross sections for the elements studied, except Fe^{54}, Ni^{60}, and Ni^{62}. The large cross sections for these nuclides appear to be best explained by compound-nucleus processes.

The angular distribution of deuterons and protons from the $Be^9(\alpha,d)B^{11}$ and $Be^9(\alpha,p)B^{12}$ reactions, leading to definite states of B^{11} and B^{12}, can be fitted reasonably well by Butler's theory.

MECHANISMS OF THE (α,pn) REACTION

Robert Joseph Silva

Lawrence Radiation Laboratory and Department of Chemistry
University of California, Berkeley, California

March 1959

I. INTRODUCTION

There has been a good deal of speculation as to the mechanism of the nuclear reaction involving the bombardment of nuclei with helium ions accelerated up to some 50 Mev to form product nuclei which have an atomic number one unit higher and a mass number two units higher than the target nuclei, i.e., the (α,pn) reaction. The work of Ghoshal,[1] which has long been cited as confirmation of the Bohr compound-nucleus model[2] of nuclear reactions, includes the reaction $Ni^{60}(\alpha,pn)Cu^{62}$. According to the statistical theory,[3] which is an extension of the original Bohr concepts, this reaction would proceed by the incorporation of the bombarding helium ion into the target nucleus to form an excited "compound" nucleus, which then de-excites by "evaporation" of particles after a time that is several orders of magnitude longer than the time of traversal of the nucleus by a helium ion. However, radiochemical cross-section investigations of the (α,xn) and (α,pxn) reactions made in the heavy-element region have led others[4,5,6] to postulate that the heavy-element reactions involving the emission of charged particles proceed by direct-interaction mechanisms between the bombarding helium ions and the target nuclei, such as those described by Butler[7] and Serber.[8]

Their experiments, as well as similar experiments[9] in which medium and heavy elements were bombarded with neutrons, protons, and gamma rays, show a much larger charged-particle emission probability than would be expected from the statistical model. Eisberg, Igo, and Wegner[10] found that, the differential cross section for the production of low-energy protons in the bombardment of copper, gold, and aluminum with 40-Mev helium ions does not vary with the center-of-mass angle in

the vicinity of 150°, which is in accord with statistical theory. However, the differential cross section for high-energy protons decreases with increasing angle, which is characteristic of optical-model direct interactions.[9] Finally, a recent survey of tritium production in various elements across the periodic table has shown that (α,t) stripping is a prominent reaction and constitutes practically all of the (α,p2n) reaction in the heavy elements.[11] It has been suggested that the (α,pn) mechanism involves either the prompt emission of a deuteron, leaving the residual nucleus insufficiently excited to emit any more particles, or the prompt emission of a proton, leaving the residual nucleus just sufficiently excited to evaporate only one neutron.[4,5]

This incestigation was undertaken to try to determine which of the afore mentioned processes are taking place and to what extent they contribute to the total (α,pn) reaction cross section. It was felt that a general survey of the (α,pn) reaction cross section across the periodic table would be valuable in showing any trends or possible changes of mechanisms. Radiochemical excitation functions have been reported for this reaction on Ni^{60},[1] Bi^{209},[12] U^{238},[5] Th^{232},[4] Pu^{238},[6] and Cf^{252}.[13] The cross section for the production of only the long-lived isomer of a pair was determined for bismuth, uranium, and thorium, while only the short-lived isomer was measured for californium.[14] These (α,pn) excitation functions have been recorded in Fig. 1 along with some unpublished data for Fe^{54},[15] and for Pt^{198}.[16] In order to make this radiochemical survey more complete, the excitation functions for the (α,pn) reaction of the targets Ni^{62}, Se^{80}, Pd^{110}, and La^{139} were obtained and are presented in a later section. Because of the unusually large cross section for this reaction on Ni^{60}, a few check points near the maximum in the excitation functions were obtained and are shown in Fig. 1.

---

14. Recent experimental work has shown that the ratio of the formation of the 36-hour isomer of E^{254} to the long-lived isomer is greater than seven, (Torbjørn Sikkeland, Lawrence Radiation Laboratory, private communication, Nov. 1958).

A study of the energy spectra and angular distributions of the deuterons and protons produced in helium-ion bombardments of some of the elements studied radiochemically should enable one to distinguish between the proposed mechanisms for this reaction. Comparison of the radiochemical cross sections with cross sections for the production of deuterons and protons of selected energy ranges should give an indication of the contribution of these mechanisms. These data were obtained for Be^{9}, Al^{27}, Ni^{60}, Pd^{110}, Bi^{209}, and U^{238} from scattering-chamber experiments, and are presented in later sections.

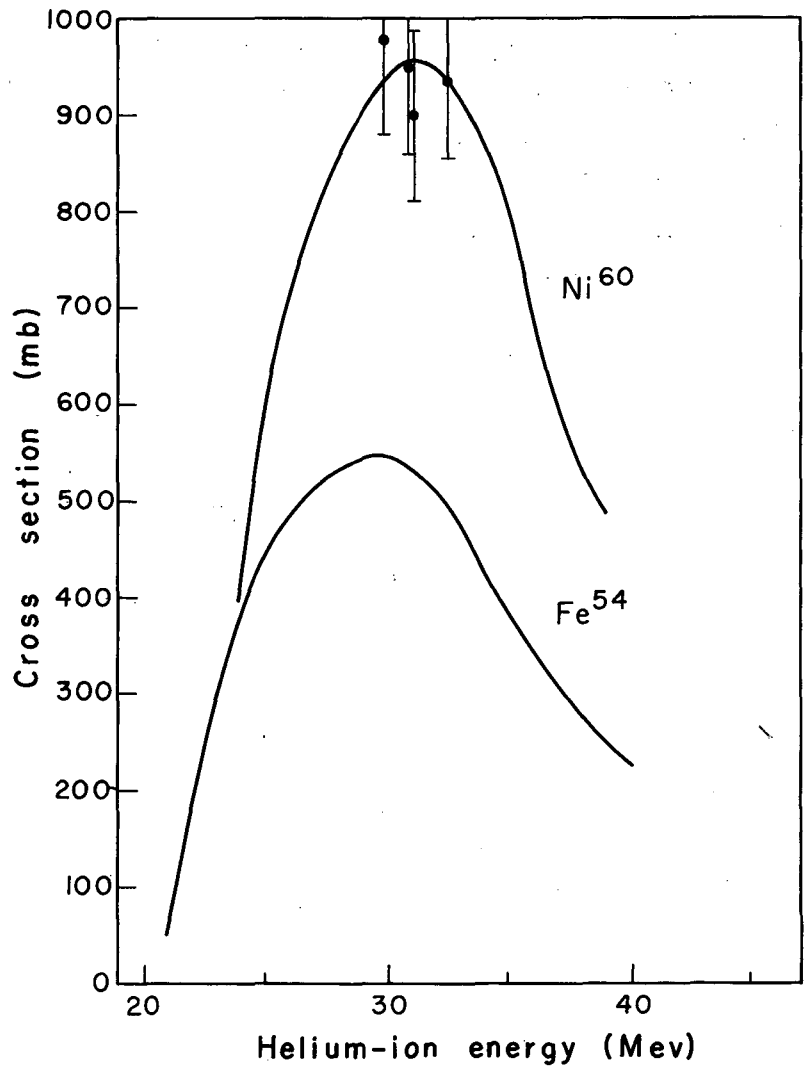

MU-16976

Fig. 1-a. Reported excitation functions for the (α,pn) nuclear spallation reaction for Fe^{54} and Ni^{60}.

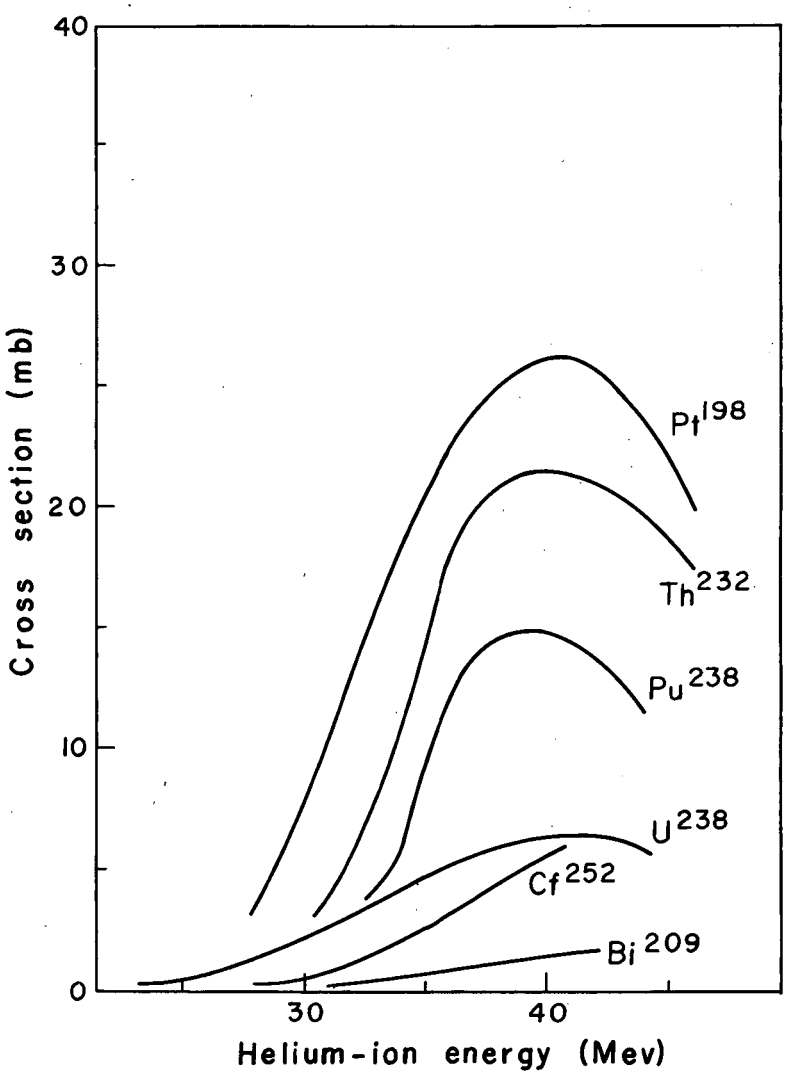

MU-16977

Fig. 1-b. Reported excitation functions for the (α,pn) nuclear spallation reaction for Pt^{198}, Bi^{209}, Th^{232}, Pu^{238}, U^{238}, and Cf^{252}.

II. EXPERIMENTAL PROCEDURES

Radiochemically Determined Cross Sections

A. Target Assemblies and Cyclotron Irradiations

All the cross-section work presented in this series of experiments was done using the 48-Mev helium-ion beam of the Crocker Laboratory 60-inch cyclotron. Two types of target assemblies were used with the external beam. A "microtarget" assembly, described fully by Ritsema,[17] was used for the palladium, selenium, lanthanum, and Ni^{62} bombardments; the stacked-foil method of target assembly was used. The beam was collimated with a 1/4-inch carbon collimator so that all the beam area fell upon target material. The range-energy curves of Aron, Hoffman, and Williams[18] were used to calculate the helium-ion energies at each target in a stack. These curves were interpolated for platinum and gold by Foreman.[19] Uncertainty in the initial beam energy due to changes in ion source and deflector and magnet settings was about ± 1 Mev. Beams of 10 to 30 $\mu a/cm^2$ were used.

A "recoil" assembly block described by R. Vandenbosch[20] was used for the Ni^{60} bombardments; however, the recoil technique was not used. The target was placed facing the beam rather than facing away from the beam, as in the recoil method. This assembly was used only because it is possible to remove the target in less than one minute, whereas the "microtarget" assembly requires several minutes. As Cu^{62} has a half-life of 10 minutes, rapid removal of the target was very important.

B. Target Preparation

1. Nickel-60

One-centimeter-diameter targets were prepared by electrodeposition of 100 $\mu g/cm^2$ of Ni^{60} onto 0.0005-inch gold foils by use of standard plating equipment.[21] The isotopic purity of the Ni^{60} was stated to be 99.1%.[22] The procedure was to dilute 10 microliters of a stock solution of Ni^{60} to 2 milliliters with a 0.5 M H_2SO_4–0.5 M HCl solution. This solution had its pH adjusted to 5 to 6 with NH_4OH, and contained 20 milligrams of

of H_3BO_3. This gave a plating solution similar to that described by Blum and Hogaboom.[23] Electroplating for 20 to 30 minutes at a current density of 100 ma/cm^2 gave consistent yields of more than 95%. The plating yield was determined by precipitation of the nickel remaining in the plating solution with dimethylglyoxime by a standard procedure[24] and comparison with standard solutions. Uniformity of the electrodeposition by this method was checked by making three platings of nickel solutions containing a small amount of mixed nickel activity produced in an alpha bombardment of natural nickel (α,αxn). The targets were checked by moving a lead absorber with a hole in it over the surface of the sample and counting the exposed activity with a proportional counter.

2. Nickel-62

Nickel-62 targets were prepared similar to those used in the Ni^{60} bombardments and by the same methods. The targets were from 200 to 300μg/cm^2. The isotopic purity was stated to be 96.8%.[22]

3. Selenium-80

Selenium targets were prepared by vacuum vaporization of analytical-grade selenium metal powder[25] from an electrically heated tantalum filament onto several weighed aluminum plates. The tantalum filament was in the form of a crucible 1 cm long, 5 mm wide, and 2.5 mm deep. The aluminum disks were placed at a distance of 20 cm from the filament, and thus the collection yield was very low (< 1%). The amount of selenium deposited was determined by weighing, and ran from 1 to 1.5 mg/cm^2. As any one disk represented less than 1% of the total collecting surface and as adjacent samples weighed very nearly the same, the targets were estimated to be uniform within 5 to 10%.

4. Palladium-110

Natural palladium foils[26] 0.00005 inches thick were used as targets for the determination of the (α,pn) cross section for Pd^{110}. The thickness of the foils was determined by weighing. The isotopic purity was taken as the natural abundance, 11.8%.

5. Lanthanum-139

Lanthanum targets were obtained by vacuum vaporization of powdered LaF_3, prepared from La_2O_3,[27] onto weighed platinum disks, by techniques described previously. In order to conserve material it was necessary to "collimate" the vaporizing LaF_3 by using a 1-cm-deep tantalum crucible and to place the disk about 6 cm away from the filament. The amount of LaF_3 deposited was about 200 $\mu g/cm^2$, which represented a 10% yield. The uniformity of the targets prepared by this method was checked by coprecipitation of a small amount of stable europium containing a mixture of radioactive Eu^{152}, Eu^{154}, and Eu^{155} with LaF_3. Four samples were prepared as described above and the uniformity was checked by scanning the surface of the sample in a manner similar to that used for Ni^{60}. This method showed that the targets had consistently 10 to 20% more LaF_3 deposited on the center area than the edges. The 6-cm distance was a compromise between yield and uniformity of target.

C. Chemical Separations

1. Nickel-60 Bombardment

As the (α,pn) product Cu^{62} has only a 10-minute half life, a rapid method of separation was desired. The following method gave separation times of about 10 minutes and yields of 50 to 60%.

After alpha irradiation, the nickel targets were dissolved in 0.5 ml hot 6M HCl containing a few drops of concentrated HNO_3, 1 mg of zinc holdback carrier, and 10 mg of copper carrier (the copper carrier was also used for yield determination). The solution was passed through a Dowex A-1 anion-exchange resin column 10 cm long and 5 mm in diameter. The resin was washed with 3 ml of 6 M HCl to elute the nickel and some other contaminents. The copper was washed from the resin with 2 ml of 2 M HCl. Gold from the target backing and zinc remained on the column. The copper solution was diluted to 1 N in HCl, a few mg of Na_2SO_3 added, and the solution heated for 1 to 2 minutes to reduce the Cu^{++} to Cu^{+}. Then 2 or 3 of 1 N NaSCN was added, which caused the precipitation of CuSCN. The precipitate was washed twice with water and dissolved in 0.5

ml of 6 M HNO_3. The solution was diluted to 2 ml with a 0.1 M HNO_3-0.1 M H_2SO_4 solution and placed in a glass plating cell.[21] The copper was plated onto a weighed platinum disk by using a current density of 0.5 amp/cm^2 for a time of 2 minutes. The copper was ignited to form CuO, and the yield was determined by weighing. The total elapsed time from cyclotron beam-off to counting was from 15 to 20 minutes.

2. Nickel-62 Bombardments

The same procedure was used for separation of copper as in the Ni^{60} bombardments. In this case, it was possible to run the columns much more slowly (resulting in better separation) and to do three separate CuSCN precipitations. The time of separation was about 3/4 hour and yields were from 65 to 80%. The higher yields were due mainly to longer plating times of from 5 to 10 minutes.

3. Selenium Bombardments

Bromine-82 was isolated from the target material by the following procedure. The selenium targets were dissolved, with slight heating, in 5 ml of 6 M HNO_3 containing 10 mg of bromine ion as KBr. A trace of fluoride ion was added to accomplish rapid dissolution of the aluminum backing. The dissolution was carried out in an airtight Erlenmeyer flask that had a glass side-arm connection which led to the bottom of a 15-ml test tube containing 10 ml each of CCl_4 and of 1 M HNO_3. When the target had dissolved, the solution was boiled vigorously and the Br_2 formed was distilled over and collected in the CCl_4 layer in the test tube. The further purification and final isolation of the bromine was accomplished by using oxidation-reduction and extraction cycles and AgBr precipitations as described by Meinke (Procedure 35-1).[28] Time of separation was about 2 hours and yields were from 30 to 50%.

4. Palladium Bombardment

The palladium foils, in which the Ag^{112} activity was induced, were dissolved in 1 ml of concentrated HNO_3 containing 10 mg of gold carrier and yield tracer. The purification of the gold was done by AgCl

and Ag_2S precipitations as described by Meinke (Procedure 47-2).[28] The final gold samples to be counted were prepared by dissolving the AgCl in 1 ml of 1 M NaCN and electroplating the gold onto weighed platinum plates. Uniform samples were obtained by using a current density of 100 ma/cm^2 for 10 minutes. The time of separation was about 2 hours and gave yields of about 50 to 60%.

5. Lanthanum Bombardment

Cerium-141 was isolated from the target material by the following procedure. After irradiation, the lanthanum targets were dissolved in 6 M HCl containing 10 mg of cerium for carrier and yield determination, 10 mg of lanthanum holdback carrier, and a few drops of concentrated HNO_3. The solution was passed through a Dowex A-1 anion-exchange resin column 10 cm long and 5 mm in diameter to remove the large amount of platinum backing material. The further purification and final isolation of the cerium was accomplished by a method described by Meinke (Procedure 58-1).[28] The time of separation was 2 hours, and the yields were from 50 to 80%.

D. Counting Instruments, Counting Technique, and Treatment of Data

1. Palladium Bombardment

The disintegration rates of the Ag^{112} samples were obtained by counting the 4.1-, 3.5-, 2.7-, and 1-Mev β^- particles using end-window gas-flow proportional counters (93% argon-7% methane) and standard scalers. The factors entering into the conversion from counts per minute to absolute disintegrations per minute are expressed in the equation

$$d/m = \frac{c/m \times A\text{-}W}{BS \times SSSA \times g},$$

where A-W is the air-plus-window absorption correction, BS the back-scattering correction, SSSA the self-scattering-self-absorption correction of the sample, and g the geometry factor. Barr has determined this total conversion factor for various self settings for the same counters used in

this experiment by counting the 1.39-Mev β^- of Na^{24} produced in a 20-mg/cm^2 aluminum target.[29] These factors were determined for thick aluminum backing plates. The palladium samples had a thickness of about 5 mg/cm^2. The use of Barr's factors could result in errors of about 10% due to the different SSSA correction as estimated from the data of Nervick and Stevenson.[30] Decay was followed on the samples for several days and the Ag^{112} activity obtained from resolution of decay curves.

2. Nickel-60 Bombardment

The disintegration rates of the Cu^{62} samples produced by short irradiations were determined by two methods: (a) counting directly the 2.9-Mev positrons emitted in the decay, and (b) counting the radiation produced by the annihilation of the positrons.

The counting of the annihilation radiation was accomplished by using a 100-channel Penco pulse-height analyzer,[31] which utilized as a detector a 1-1/2-inch by 1-inch-diameter thallium-activated sodium iodide scintillation crystal connected to a photomultiplier tube. An Am^{241} standard was used to determine the geometry of the particular shelf used, and the results of Kalkstein and Hollander[32] were used to correct for the variation in photopeak counting efficiency with gamma-ray energy.

The 2.9-Mev positrons were counted by using a proportional counter described previously; 800 mg/cm^2 of aluminum absorber was used to cut out all beta activities of energies less than about 2 Mev. The total conversion factor for the particular shelf used was obtained by using a Zn^{62} sample which was isolated from a Ni^{60} target after a 3-hour irradiation with helium ions. The disintegration rate of the Zn^{62} sample was determined (a) by following the decay of the annihilation radiation of its own positron decay and the positrons of the Cu^{62} daughter in equilibrium, and (b) from the characteristic 42-kev gamma ray of Zn^{62}. The Zn^{62} disintegration rates determined by these two methods agreed within 8%. All counting conditions were the same for counting of the positrons from the Zn^{62} standard as for the actual Cu^{62} samples, except for a slight difference in sample thickness which would

produce a different SSSA correction. This difference would amount to from 5 to 10% as estimated from the curves of Nervick and Stevenson.[30]

3. Nickel-62, Selenium, and Lanthanum Bombardments

The disintegration rates of the Cu^{64}, Br^{82}, and Ce^{141} samples were obtained by using the Penco and associated equipment, and methods described previously, to count the characteristic gamma rays as follows:

Cu^{64}	1.34 Mev;
Br^{82}	0.777 Mev;
Ce^{141}	0.142 Mev.

With all the samples decay was followed for a few half lives and the isotope identified by its characteristic gamma-ray energy and the observed half life of the gamma-ray peak.

The abundances of all gamma rays and beta particles emitted in the decay of the nuclides studied were taken from the compilation by Strominger, Hollander, and Seaborg.[33]

E. Cross-Section Calculations

The activity of each isotope was extrapolated to the end of the bombardment, and the number of atoms present at the end of the bombardment was calculated by using the formula

$$N = \frac{(d/m) \quad (T_{1/2})}{(0.693)\ (\text{chemical yield})}$$

The cross section (in millibarns) was then calculated from

$$\sigma = \frac{N}{n/cm^2 \quad (R)} (10^{27})$$

where N is the number of atoms produced during the bombardments, n/cm^2 is the number of target atoms per square centimeter, and R is the number of helium ions striking the target during the bombardments. If there was any appreciable decay of the atoms produced during the time of bombardment, the above formulae were put in the corresponding proper form to correct for this decay.

Scattering-Chamber Investigations

Deuteron and proton spectra and angular distributions were obtained for helium-ion bombardments of Be^9, Al^{27}, Ni^{60}, Pd^{110}, Bi^{209}, and U^{238}, by using the 36-inch scattering chamber at the Crocker Laboratory 60-inch cyclotron. In these experiments it was necessary to discriminate between the charge-1 particles and desirable to study certain energy ranges of these particles. This was accomplished by having the particle first pass through a CsI transmission crystal to measure their rates of energy loss, dE/dx, and then into a NaI crystal to measure their remaining total energy, E. Since the energy loss in the transmission counter is finite, it will be designated Δ E. The pulses obtained were then fed into an electronic particle identifier,[34] the output pulse of which is proportional to the product of the mass and the square of the charge of the particle. The final spectra were recorded on a 100-channel Penco pulse-height analyzer. A more detailed description of the equipment is given below.

A. Scattering Chamber

The chamber used was the 36-inch-diameter scattering chamber at the Crocker Laboratory 60-inch cyclotron.[35,36,37] The helium-ion beam was brought out externally through a long iron pipe and, after quadrupole focusing and collimating, impinged on a thin metal foil placed at the center of the chamber at an angle of 45° to the beam. The detector was mounted on a rotating table that comprised the bottom of the chamber and could be placed at any desired angle from 10° to 150° with respect to the beam. The intense gamma radiation, produced when the detector intercepted the helium-ion beam at angles smaller than 10°, saturated the electronic system. Beryllium degrading foils were placed just in front of the focusing magnet if a beam energy less than 48 Mev was desired. The beam intensity was measured with a Faraday cup placed at the back of the scattering chamber. The Faraday cup was provided with foil wheels containing varying amounts of aluminum absorber. The beam energy was determined by interposing just sufficient aluminum

to absorb out the beam and calculating the helium-ion energy from range-energy tables[38] based on experimental proton range-energy data.[39]

A schematic view of the apparatus is given in Fig. 2.

B. Targets

Natural foils of 0.001-inch Be^9, 0.00025-inch Al^{27}, and 0.00075-inch U^{238} were used as targets. The Ni^{60} foil was prepared by electrodeposition of nickel onto a 0.0001-inch copper backing, using a plating method described previously.* The copper was subsequently dissolved off with a 0.1 M $AgNO_3$ solution. The isotopic purity of the Ni^{60} was stated to be 87%.[22] The target prepared in this way was 0.00034 inch thick.

The Pd^{110} target was prepared by electroplating Pd^{110} onto a 0.001-inch natural palladium foil, using the method described by Blum and Hogsboom.[23] The palladium solution used was stated as having an isotopic purity of 91.7% Pd^{110}.[22] The isotopic dilution due to the natural palladium backing brought the amount of Pd^{110} in the target down to 78%; the target was 0.00038 inch thick. All the protons and deuterons were assumed to arise from the reactions of this nuclide.

The Bi^{209} target was prepared by vacuum vaporization of analytical-grade bismuth from an electrically heated tantalum filament onto an aluminum backing, using the same volatilizing methods described earlier. The aluminum was subsequencly dissolved off with dilute HCl. The bismuth target was 0.00034 inch thick.

C. Detectors

1. Δ E Counter

A schematic representation of the detector system is given in Fig. 3. The detector used for measuring the average rate of energy loss, Δ E, of a particle was a CsI crystal 10 mils thick (115 mg/cm^2) and 5/16 inch in diameter. It was coated on the back and sides with an

---

*See page 10.

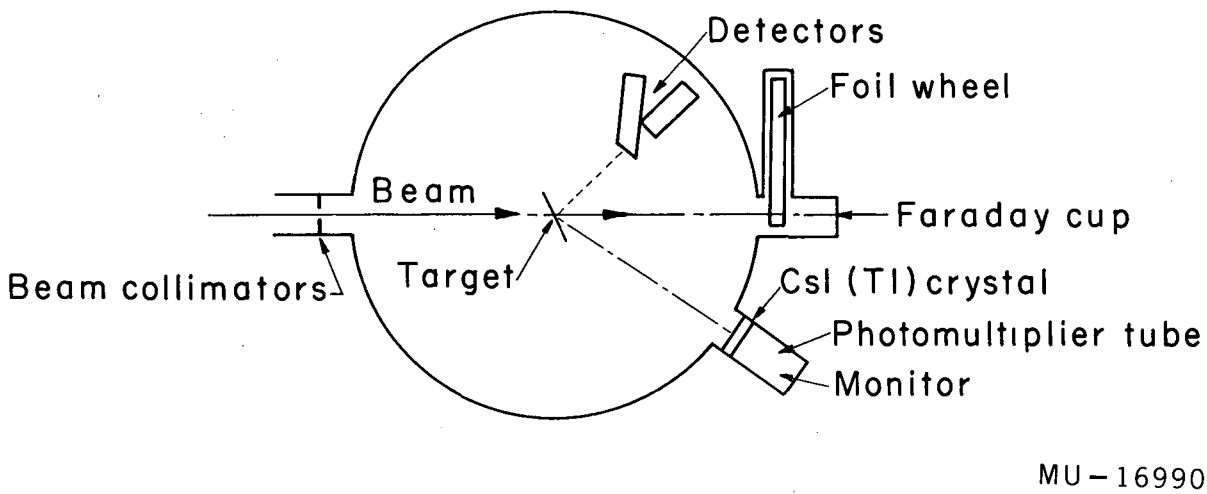

Fig. 2. Schematic diagram of scattering chamber and detector.

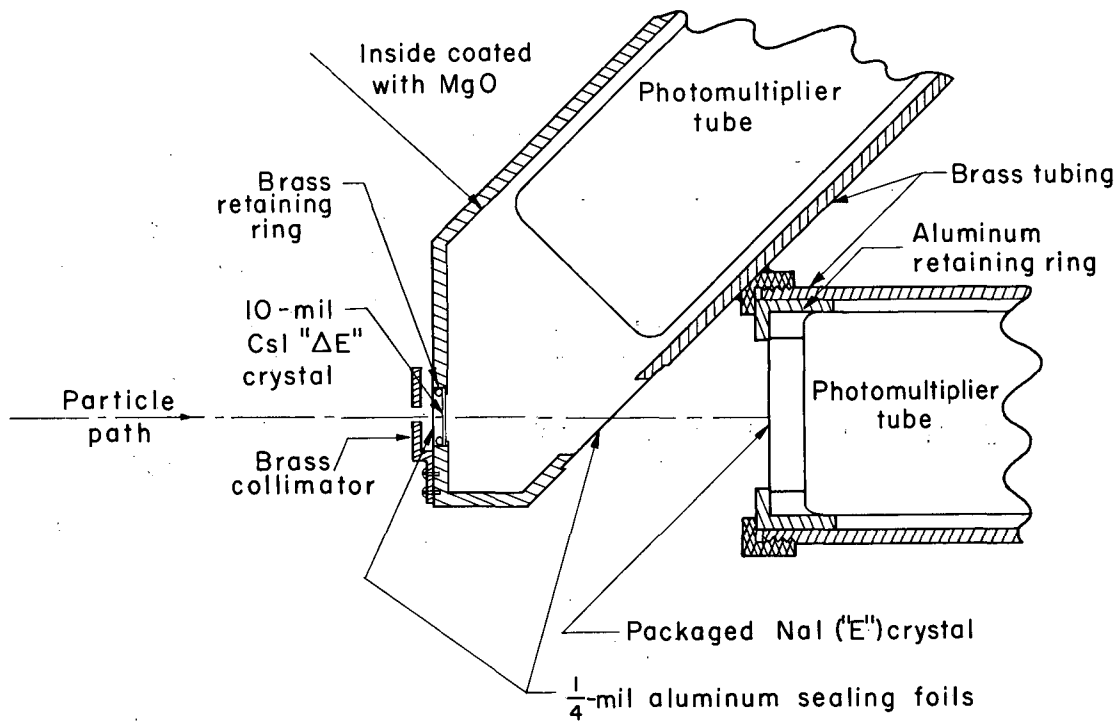

MU-16957

Fig. 3. Diagram of detector for Δ E and E.

aluminum mirror for light reflection; 24-Mev deuterons lost about 2.5 Mev when passing through the crystal. A DuMont 6292 photomultiplier tube operated at 1100 volts looked at this crystal at an angle of 45° and a distance of about 4 cm. For the bombardment of aluminum with 24-Mev deuterons, the energy spectrum of the elastic peak observed at 10° had a full width at half maximum of about 15 to 17%.

2. E Counter

The detector used for measuring the remaining energy of the particles after passage through the Δ E crystal was a thallium-activated sodium iodide crystal about 3/8 inch thick and 1 inch in diameter. The crystal was packaged in an airtight aluminum container with a transparent window. The aluminum container at the point where the particles entered was 0.00025 inch thick. A DuMont 6292 photomultiplier tube was in contact with the crystal's window and was operated at 850 volts dc. Precautions were taken against light or air leaks. For the bombardment of aluminum with 24-Mev deuterons the energy spectrum of the elastic peak observed at 10° had a full width at half maximum of about 3 to 4%.

3. Foil Wheel

A foil wheel with various amounts of aluminum absorber was placed in front of the detector crystals and could be rotated by remote control. This permitted variation of the energy of the particles being detected by the crystals. This was used to help identify energy peaks corresponding to different types of particles by measuring their energy loss in various amounts of aluminum. It was also used to cut out the helium ions elastically scattered into the detector and to help align the electronic particle identifier as described later.

A brass 1/8-inch collimator was placed in front of the foil wheel so that the detector subtended a solid angle of 1.59×10^{-4} steradians. The foil wheel could be placed between the brass collimator and the first aluminum window.

D. Electronic Particle Identifier

Ample description of the theory and operation of this electronic system has been given elsewhere,[34] therefore only a brief account is given here.

The principle of operation of this device is based on the approximate equation obtained from the nonrelativistic formula for rate of energy loss of charged particles as they pass through matter.[40] For particles of charge-1 it can be put in the form

$$\frac{de}{dx} = \frac{C_1 M}{E} \ln C_2 \frac{E}{M},$$

where M = mass of the charged particle, E = the energy of the charged particle, and C_1 and C_2 are conglomerates of the constants in the usual formula. The mass of a charged particle is proportional to the product of the rate of energy loss by the particle and its total energy. Stokes, Boyer, and Northrup[41] have shown that the effect of the log term is greatly reduced by the addition of a properly selected constant E_o to the total energy of the particle E, so that over a wide range of energies the product of $(E+E_o)$ and de/dx is closely proportional to the mass. In practice there is a finite energy loss in the CsI crystal, therefore one-half of the ΔE must be added back to the measured particle energy from the E crystal in order that E and ΔE correspond to the same particle energy. The final expression is then

$$M \sim (E + E_o + 1/2 \Delta E) \Delta E .$$

The computer circuit utilizes the ΔE and E pulses to perform the multiplication

$$(A + B)^2 - (A - B)^2 = 4 AB ,$$

where $A = E + E_o + K \Delta E$, and $B = \Delta E$. The squaring is performed by two Raytheon Q K - 329 beam-deflection tubes which utilize a specially shaped target electrode placed in the path of the electron beam. The target electrode is pierced with a parabolic aperture so that the current collected at the plate and at the target electrode is a function of the square of the deflection voltage.

The exact values of K and E_o are left as adjustable parameters. Since E_o is introduced as a dc bias on the deflectors of the squaring tubes, one can have spurious pulses appearing at the computer output. These pulses are the result of E_o multiplying the Δ E pulse of a particle or gamma ray that traverses the Δ E crystal but does not strike the E crystal. These spurious pulses are eliminated by a coincidence requirement between the E pulse and the output pulse of the pulse multiplier, as discussed later. The product pulses obtained from this electronic multiplier have an amplitude nearly proportional to the mass of the particles observed, regardless of their energies. The spectra obtained in this manner will hereafter be referred to as the particle spectra, in contrast to the actual energy spectra of the particles.

E. Pulse-Height Analyzer

The pulses from the crystals or the pulse multiplier were analyzed by use of a 100-channel Penco pulse-height analyzer.[31] This analyzer has a coincidence circuit so that signal pulses, to be acceptable, must have a corresponding trigger pulse. The gate circuit is provided with a discriminator so that pulses smaller than a definite preset value will not trigger the analyzer.

F. Alignment of the Electronic Particle Identifier

A rough alignment and a linearity check of the multiplier were first obtained following the procedure of Brisco.[34] The multiplier gave a linear response over a range of 5- to 80-volt pulses.

Rough selection of K and E_o were made by bombarding a gold foil with 24-Mev deuterons and observing the elastically scattered deuterons at an angle of 10°. The multiplier output was observed with the pulse-height analyzer and the particle spectrum consisted primarily of one peak due to E x Δ E of the elastically scattered deuterons. By means of the aluminum foil wheel in front of the detector, the energy of these elastically scattered deuterons was decreased in steps to about

7 Mev. K and E_o were adjusted in such a manner that the multiplier peak did not shift in pulse height as the energy of the elastically scattered deuterons changed. The same procedure was followed for protons. Final fine adjustment of the multiplier was made during bombardment of the actual target with helium ions while the multiplier pulses were observed with the pulse-height analyzer. Sufficient aluminum was placed in front of the detector to stop all the elastically and inelastically scattered helium ions. Three peaks were observed in the particle spectrum, corresponding to protons, deuterons, and tritons, and small changes in K and E_o were made to maximize the separation of these groups. A typical particle spectrum, obtained for aluminum + α at 15°, is shown in Fig. 4.

In order to determine if the multiplier was distorting the true counting rates of the particles observed, the number of counts in the peak of an energy spectrum obtained directly from the E crystal for elastically scattered deuterons was compared with the number of counts in the peak of the deuteron particle spectrum for equal numbers of incident beam particles. The same was done for elastic protons. The counting rates agreed within 10%. The same procedure was carried out with varying beam intensities. At counting rates actually used (less than 10^4 cpm) there was no distortion of the counting rate by the multiplier. Frequent checks were made during the series of bombardments to make sure that the multiplier and associated equipment was functioning properly.

G. Method of Operation

1. Energy Spectra

The energy spectra of protons and deuterons from the various bombardments were obtained by using the E pulse as the signal pulse to the Penco and electronic particle-identifier pulse (after proper modification) to generate a gate pulse for the Penco. A schematic diagram of the electronic circuit used is given in Fig. 5.

The pulse shaper was used to eliminate the negative half of the pulses from the Franklin DD-2 amplifier with a series-shunt diode

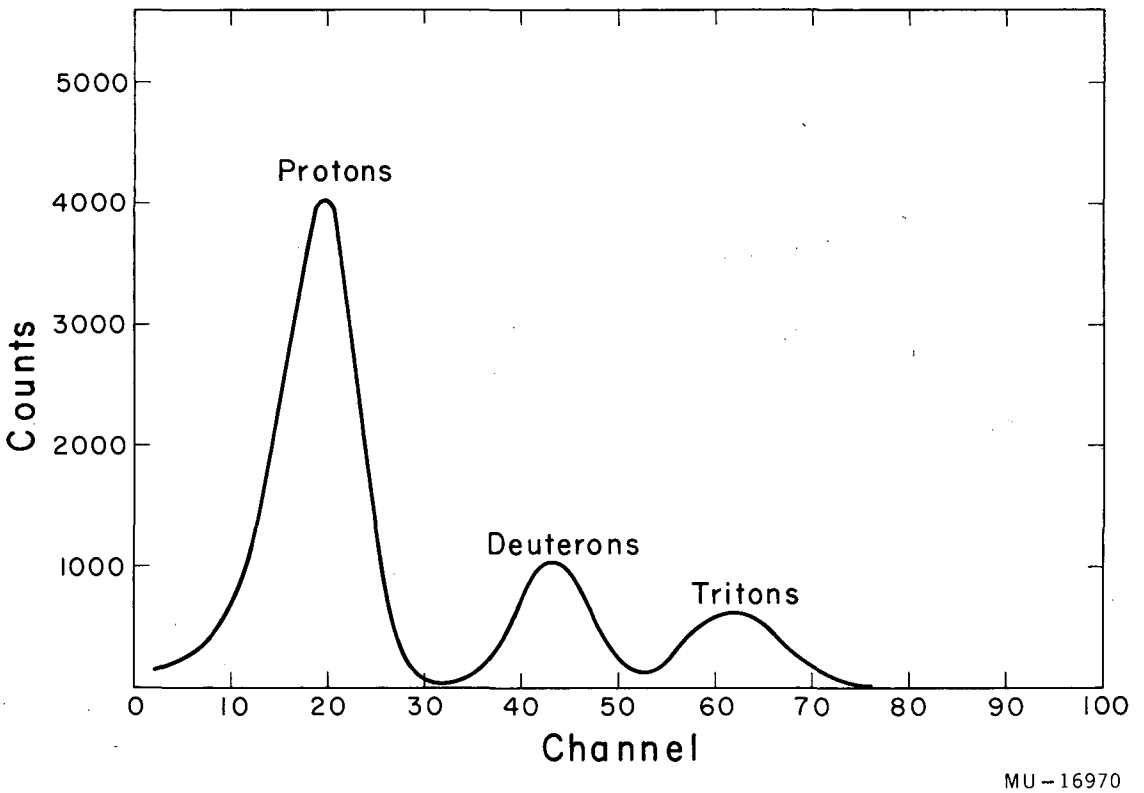

Fig. 4. Particle spectrum obtained in the bombardment of aluminum with 41-Mev alpha particles at 15 deg (lab).

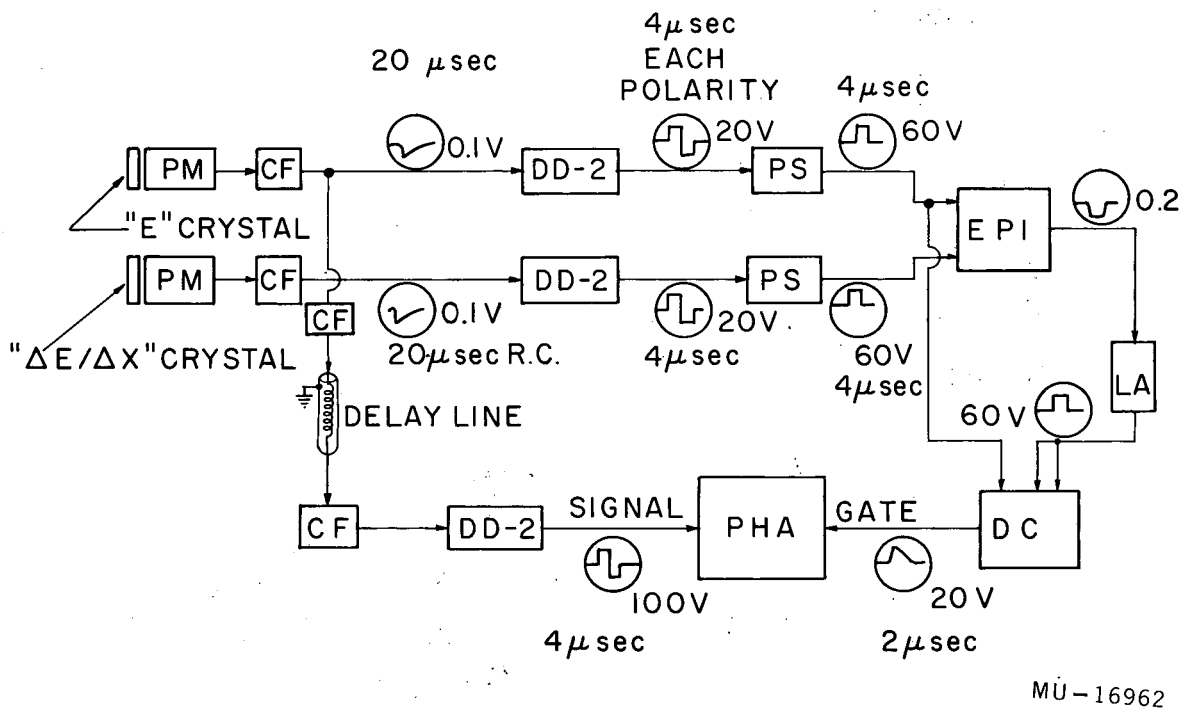

Fig. 5. Block diagram of electronic circuit used to obtain energy spectra. The pulse heights in volts and the pulse widths in microseconds are included.

network. It was also used to adjust the pulses so that they were as nearly identical as possible for pulse multiplication. An 8-microsecond delay was used in the E-pulse signal circuit to match in time the signal pulse and the gate pulse obtained from the relatively slow coincidence circuits. The rest of the electronic equipment performed its standard functions.

The coincidence circuit had variable discriminators so that only coincidence pulses were generated for incoming multiplier pulses of pulse height between adjustable upper and lower limits. An E-pulse coincidence requirement was also imposed to eliminate trigger pulses originating from spurious pulses in the multiplier spectrum.

To properly adjust the discriminators in the gate circuit for obtaining a deuteron energy spectrum, the upper discriminator window was set for a pulse height corresponding to the middle of the deuteron-triton valley and the lower discriminator window set for the middle of the proton-deuteron valley in the particle spectrum. This was easily accomplished by using the amplified particle-spectrum pulses from the multiplier as a singal, as well as a trigger pulse, and adjusting the upper and lower discriminators until only the deuteron particle peak was recorded in the spectrum of the pulse-height analyzer.

With this arrangement, only those pulses in the all-inclusive energy spectrum were recorded for which there was a coincidence pulse corresponding to a deuteron in the particle spectrum. A similar scheme was used for obtaining the proton spectrum.

In order to convert channel number to energy, it was necessary to calibrate the pulse-height analyzer and associated equipment. This was done by observing (a) the peak for elastically scattered protons arising from the bombardment of gold with 12-Mev protons, and (b) the proton groups leading to the ground and first excited states of Be^{10} arising from $Be^{9}(d,p)Be^{10}$ reaction. The beryllium reaction has been studied quite extensively and the Q values corresponding to these groups are well known.[42] The protons detected from both bombardments were degraded in energy step by step with the aluminum foil wheel in front of the detector. It was possible to obtain a well-defined calibration curve

running from 5 to 28 Mev. All points fell within 1 Mev of the best straight line through the points. Several such curves were obtained for different amplifier settings used. Check points were taken before and after each series of angular measurements. Corrections were made for any slight shifts due to small changes in photomultiplier or amplifier voltages.

2. Particle Spectra

The particle spectra could be obtained simply by using the amplified output of the particle identifier directly as a signal pulse. In order to eliminate spurious multiplied pulses that did not correspond to any E pulse, the E pulse was used as a gate pulse. The discriminator in the Penco gate circuit could be used to set a lower limit to the energy of the particles recorded. The Penco discriminator circuit was calibrated by observing at 15° the elastically scattered deuterons obtained from the bombardment of gold with 24-Mev deuterons. The energy of the peak for elastically scattered deuterons could be changed by using the aluminum absorber foil wheel in front of the detector, and the discriminator setting just necessary to reject the elastic peak recorded. Other energy settings could be obtained by interpolation with an estimated error of ± 1 Mev.

III. RESULTS

A. Radiochemically Determined Cross Sections

The excitation functions for the (α,pn) spallation reaction on Ni^{62}, Se^{80}, Pd^{110}, and La^{139} for helium-ion energies up to 48 Mev are presented in Fig. 6. The cross sections determined for Ni^{60} are compared with Ghoshal's curve in Fig. 1. The errors shown were estimated for each on the basis of uncertainties in target thickness, counting efficiencies and geometries, and resolution of gamma-ray peaks and decay curves. Probable errors due to counting statistics were usually less than 1%. The estimated errors are as follows:

Ni^{60}	±	10%
Ni^{62}	±	15%
Se^{80}	±	15%
Pd^{110}	±	20%
La^{139}	±	15%

The errors listed are relative errors for each set of data. Any changes in the listed abundances of the gamma rays or beta particles detected accordingly changes the absolute values. The errors in the listed abundances are low except for Ni^{62}, where there could be an uncertainty of as much as ± 30% in the abundance of the 1.34-Mev gamma ray used to determine the disintegration rate.

B. Scattering-Chamber Studies

1. Introduction

Energy spectra and angular distributions of deuterons and protons emitted during the bombardment of Al^{27}, Ni^{60}, Pd^{110}, Bi^{209}, and U^{238} with helium ions of 41 and 48 Mev were obtained. In light nuclei, the nuclear levels near the ground state may be separated by several Mev. Reactions leading to these states produce groups of particles of discrete energies. As the angular distributions of protons and deuterons leading to separate levels are of considerable theoretical interest, energy spectra were obtained at a helium-ion bombarding energy of 48 Mev for Be^{9}.

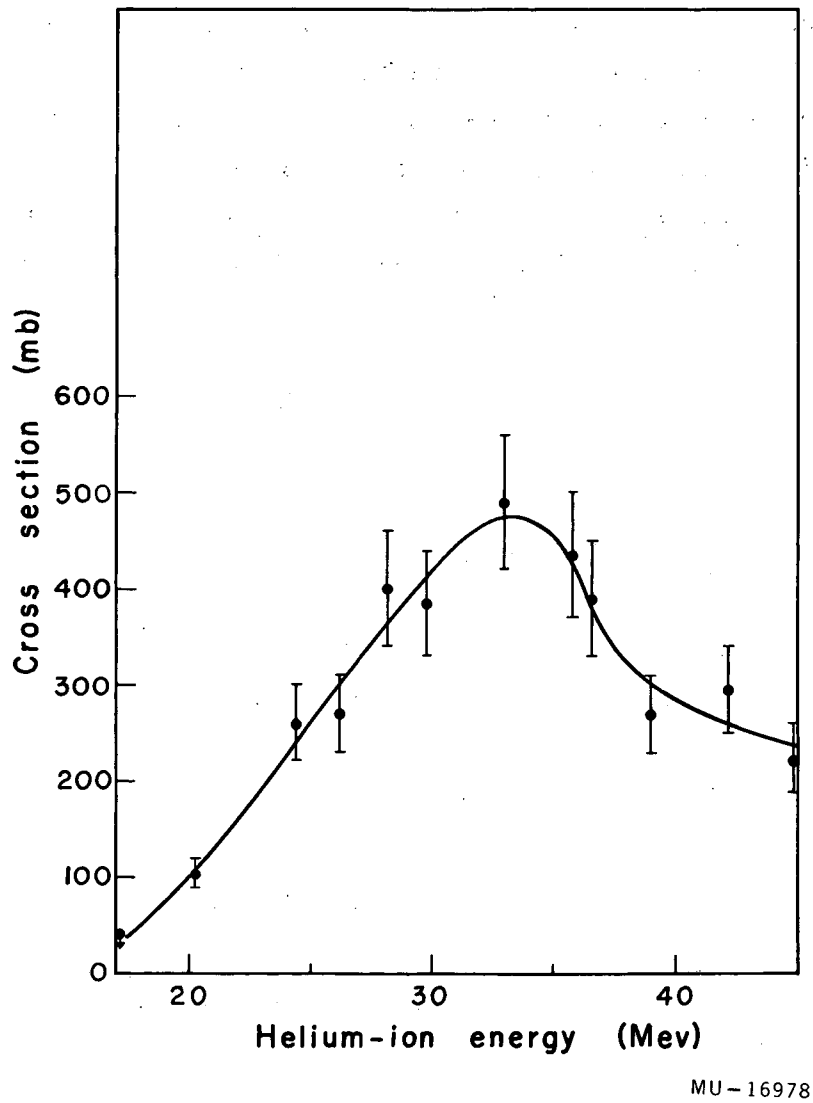

Fig. 6-a. Spallation excitation function for the (α,pn) reaction of Ni^{62}.

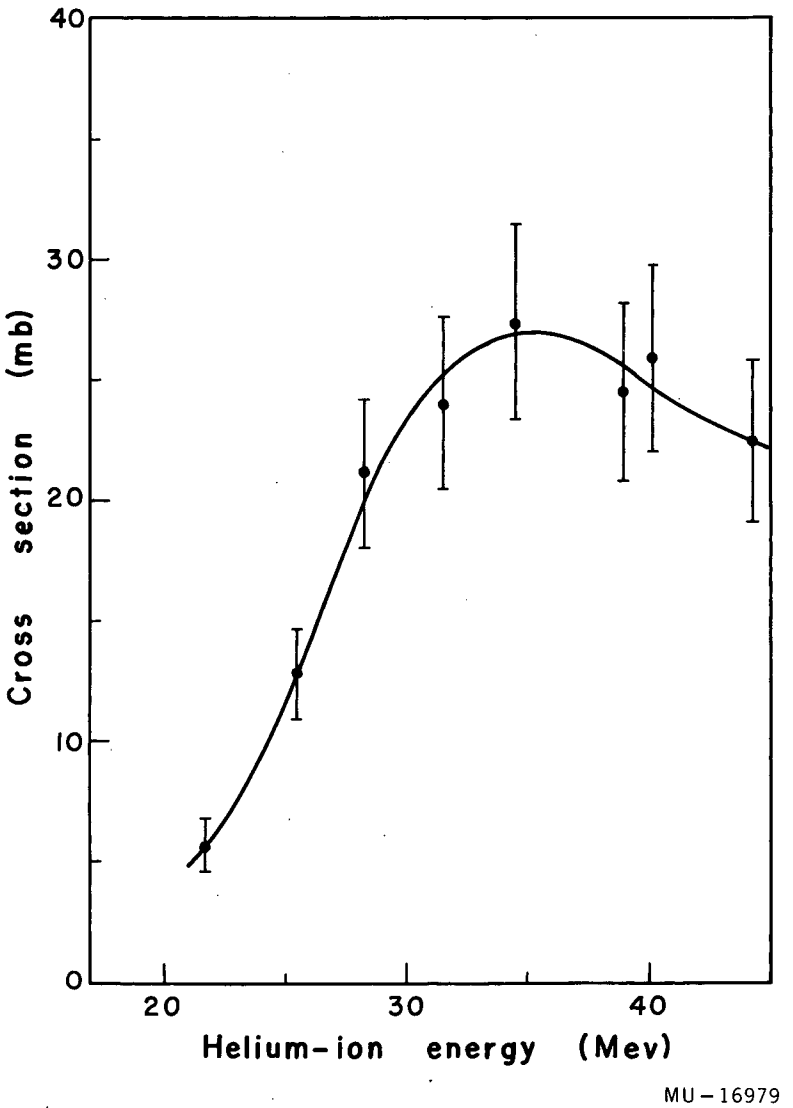

Fig. 6-b. Spallation excitation function for the (α,pn) reaction of Se^{80}.

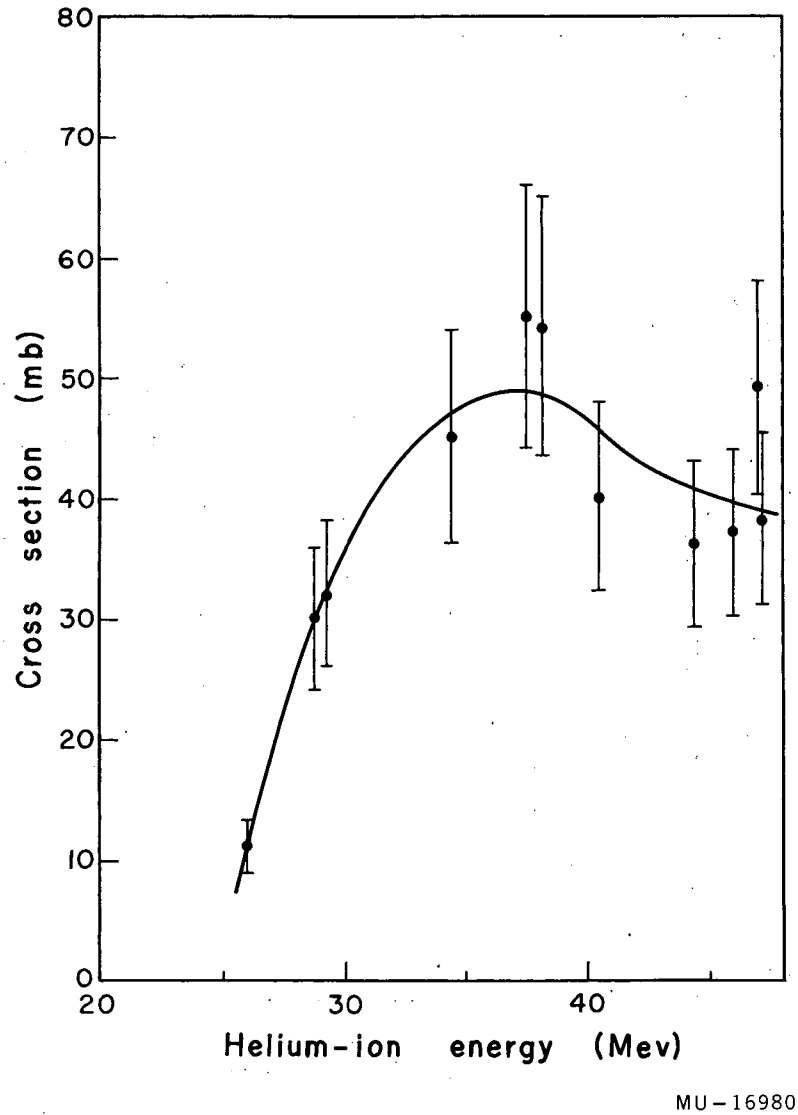

Fig. 6-c. Spallation excitation function for the (α,pn) reaction of Pd^{110}.

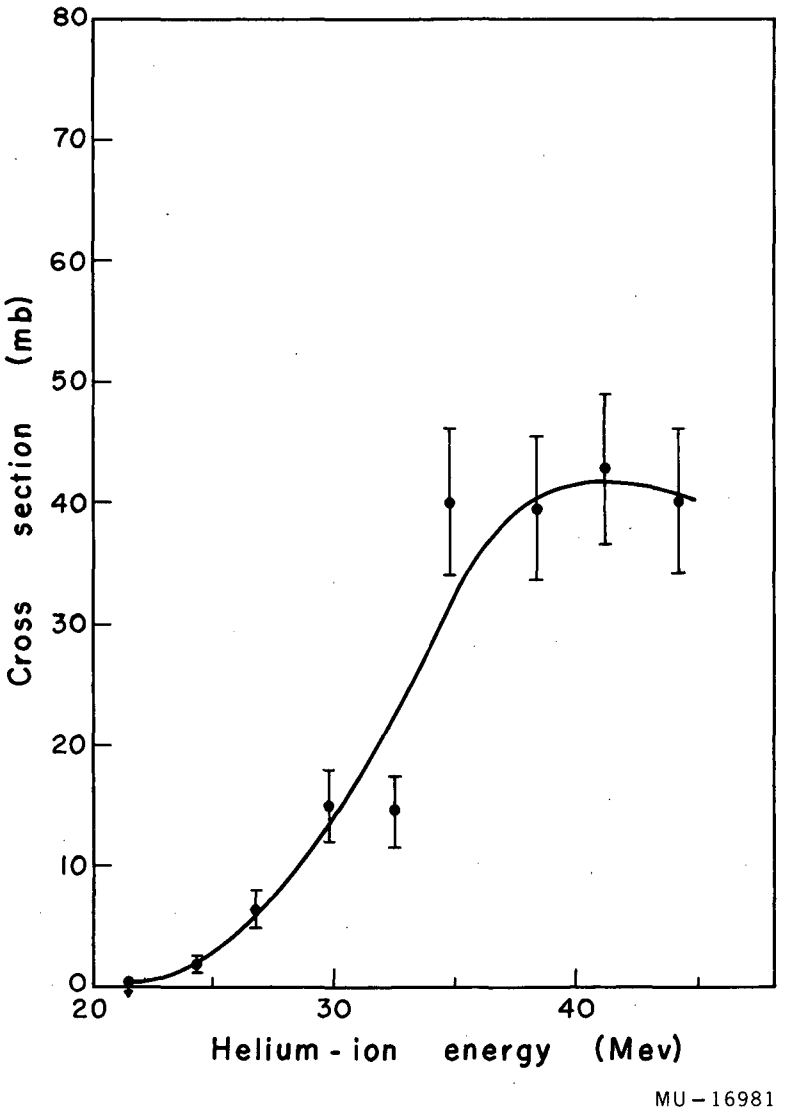

Fig. 6-d. Spallation excitation function for the (α,pn) reaction of La^{139}.

Because of the high intensity and large energy loss in the crystals, the elastically scattered helium ions present in the bombardments completely saturated the electronic system and caused the amplifiers to "limit" at gain settings desirable for proton and deuteron study. It was therefore necessary to place sufficient aluminum in front of the detector to absorb all the helium ions. At bombarding energies below about 40 Mev,* some protons and deuterons that were considered to be contributing to the (α,pn) radiochemical cross sections (i.e., α,d plus α,pn), were also being absorbed. This was because the protons and deuterons had to pass through the Δ E crystal (an additional 115 mg/cm^2 of CsI) to reach the E crystal. As the energy of the bombarding particles was lowered, the 115 mg/cm^2 of CsI became an increasingly larger fraction of the range of the protons and deuterons emitted from nuclear reactions. When bombarding with 48-Mev helium ions, the low-energy cutoff for protons was about 15 Mev and for deuterons about 20 Mev. Unfortunately this energy limit eliminated the possibility of bombarding at lower helium-ion energies, where the maxima, attributed to compound-nucleus mechanisms, occur in the light-element radiochemical excitation functions.

2. Deuteron Energy Selection

In order to obtain the cross section for the production of deuterons corresponding to the (α,d) reaction only, and not this reaction followed by the emission of other particles, it was necessary to adopt a scheme for selecting from the entire deuteron-energy distribution the deuterons whose energies were most probably associated with this reaction. This was done by placing an energy restriction on the particles selected, based on assumptions about the kinetics of the reactions. The assumption was made that deuterons would be considered to contribute to only the (α,d) reaction when their observed energy corresponded to a

---

*It was possible to obtain some points for Al^{27} at an alpha energy of 34 Mev, because of the relatively low Q values involved.

deuteron emitted first and leaving a residual nucleus with an excitation energy of less than the binding energy of the last, least bound particle. In all the elements bombarded except Ni^{60}, the binding energy of the last neutron to the product nucleus from (α,d) reaction is less than that of the last proton. The binding energy of the proton in Cu^{62} is about 2 Mev less than the neutron. However, evaporation of "slow" protons* supposedly does not compete favorably with gamma-ray emission until the nuclear excitation energy is about 2 Mev greater than the binding energy of the proton.[43,44] Therefore "slow" proton emission and neutron emission would appear at about the same nuclear excitation in Ni^{60}. The assumption was that whenever the observed deuteron energy was low enough to leave the residual nucleus excited to the binding energy of a neutron, a neutron would be emitted and the reaction would then no longer contribute to the (α,d) reaction as defined. The acceptable energy range for deuterons was taken as

$$E_\alpha + Q_{\alpha,d} > E_d > E_\alpha + Q_{\alpha,dn},$$

where Q is the energy release in a given reaction. This analysis was not made for Be^9.

3. Deuteron Cross Sections

The deuteron differential cross sections for Al^{27}, Ni^{60}, Pd^{110}, Bi^{209}, and U^{238} were obtained from the proton-deuteron-triton particle spectra (with the proper selection of energy) rather than from the deuteron energy spectra. This method was felt to yield more reliable cross sections than could be obtained from the deuteron energy spectra. During the early development of the particle-identification system, the separation of the deuteron peak from protons and tritons in the particle spectra was not considered good enough to eliminate contamination of the deuteron energy spectra. With improved resolution, there was still appreciable triton contamination in the bismuth and uranium bombardments, for in these cases the triton particle peak was considerably higher than

*Protons of energy considerably less than the Coulomb barrier.

the deuteron peak. However, it was possible to resolve the deuteron particle peak from the proton and triton peaks with some confidence, as the particle peaks were fairly symmetric about their maxima.

Only deuterons whose energies were above the energy limit assumed for deuterons associated with only the (α,d) reaction were included in the particle spectra. This was done using the calibrated discriminator in the Penco gate circuit. Checks were made on the discriminator calibration, using elastically scattered deuterons, before each series of angular measurements.

The variation of the differential cross sections with angle for the production of deuterons leading to the (α,d) reaction for aluminum, nickel, palladium, bismuth, and uranium are presented in Table I. Also listed in Table I are the total cross sections obtained from an integration of these angular distributions. As the differential cross sections continued to decrease with increasing angle, it was not felt worth while to go to larger angles, because the counting time was quite long. This amounts to an estimated elimination of less than 5% of the total cross sections.

The total cross sections were obtained by integration of the angular distribution curves according to the equation

$$\sigma = 2\pi \int_0^{\pi} \frac{d\sigma}{d\Omega} \sin\Theta d\Theta .$$

In practice the integral was approximated by a summation. The graphical integration was carried out step-wise in 5° intervals by using the average values of $\frac{d\sigma}{d\Omega}$ and $\sin\Theta$ for that interval. The angular distribution of deuterons from the $Be^9(\alpha,d)B^{11}$ reaction, leading to the ground and first excited states of B^{11}, were obtained from the deuteron energy spectra when the resolution of the particle spectra was improved. Less than 10% of the counts in the deuteron particle peak might be attributed to protons or tritons. The angular distributions of deuterons leading to these states in B^{11} are also given in Table I.

Table I

Deuteron differential cross sections as a function of laboratory-system angle for helium-ion bombardment at 34, 41, and 48 Mev (millibarns/steradian)

Angle (lab system) (degrees)	Isotope												
	Al^{27}			Ni^{60}		Pd^{110}		Bi^{209}		U^{238}		Be^{9}	
	34 Mev	41 Mev	48 Mev	41 Mev	48 Mev	41 Mev	48 Mev	41 Mev	48 Mev	41 Mev	48 Mev	48 Mev Ground state	48 Mev 1st excited state
10			5.45±0.54										
12.5					8.38±0.84	5.13±1.02	6.96±0.84					2.34±0.19	0.883±0.132
15	5.39±0.75	5.85±0.39	3.49±0.24	5.01±0.60	6.60±0.53	4.28±0.63	4.80±0.48	1.66±0.33	2.39±0.48	4.19±0.76	5.96±1.80	1.43±0.080	0.889±0.090
20	3.90±0.39	4.23±0.33	2.60±0.21	3.52±0.53	4.60±0.37	3.29±0.48	4.02±0.41	1.07±0.21	1.90±0.38	3.34±0.66	4.45±0.53	0.926±0.047	0.586±0.059
25	2.58±0.15	2.92±0.27	1.84±0.18	2.13±0.26	3.22±0.26	2.25±0.22	3.46±0.35	0.93±0.19	1.15±0.23	1.52±0.44	3.18±0.47	0.780±0.042	0.416±0.042
30	1.68±0.15	2.25±0.18	1.34±0.12	1.68±0.34	1.75±0.18	1.77±0.18	2.55±0.24	0.74±0.15	0.99±0.20	0.76±0.38	1.93±0.29	0.898±0.048	0.236±0.024
35	1.24±0.12	1.76±0.15	1.14±0.11			1.26±0.13	1.86±0.19			0.60±0.20	1.35±0.33	0.933±0.065	0.260±0.026
40	0.91±0.09	1.56±0.15	0.91±0.09	0.76±0.11	1.37±0.14	0.91±0.09	1.61±0.16	0.42±0.08	0.57±0.11	0.38±0.13	0.83±0.29	0.720±0.050	0.255±0.026
45		1.13±0.11	0.82±0.15								0.61±0.20	0.522±0.042	0.182±0.025
50	0.56±0.09	0.85±0.09	0.56±0.11	0.62±0.09	0.77±0.08	0.52±0.06	0.74±0.09	0.23±0.05	0.35±0.07	0.19±0.09	0.70±0.15	0.388±0.038	0.118±0.025
55			0.45±0.05										
60	0.51±0.09	0.61±0.06	0.35±0.05	0.31±0.05	0.42±0.04	0.30±0.04	0.39±0.05	0.15±0.03	0.18±0.04	0.12±0.06	0.35±0.13	0.320±0.048	0.078±0.023
70	0.44±0.09	0.42±0.08	0.28±0.04	0.22±0.05	0.24±0.02	0.18±0.03	0.17±0.02	0.10±0.02	0.11±0.02			0.196±0.040	0.050±0.020
80		0.23±0.09	0.16±0.03	0.14±0.03	0.17±0.02	0.11±0.02	0.12±0.02	0.06±0.02	0.07±0.02	0.05±0.02	0.11±0.04	0.126±0.038	
90	0.37±0.08		0.14±0.03			0.08±0.02	0.07±0.02					0.112±0.044	
100		0.25±0.11		0.06±0.02	0.06±0.01			0.02±0.006	0.02±0.006		0.03±0.01		
110			0.08±0.03				0.03±0.01						
Total cross section (mb.)	6.50±1.63	7.95±1.39	5.14±0.77	5.57±0.95	7.49±0.85	5.57±0.79	6.84±0.96	2.18±0.76	2.93±0.65	3.42±1.36	6.18±1.85		

Figure 7 shows some typical energy spectra obtained for beryllium, aluminum, and palladium. Figure 8 shows angular distributions of deuterons for the (α,d) reaction on aluminum and palladium. The other elements studied gave very similar results. Figure 9 shows plots of the variation of the differential cross sections with center-of-mass angle for the Be^9(α,d) reaction leading to the ground and first excited states of B^{11}, together with theoretical curves calculated by using Butler's theory[45] as described below.

The errors listed were estimated from uncertainties in target thicknesses, energy calibrations, and resolution of the particle spectra peaks. Errors due to counting statistics were usually small except at very large angles. The errors listed for the Be^9 bombardments are relative errors estimated from resolution of energy-spectra peaks and counting statistics.

4. Proton Energy Selection

The deuteron cross sections obtained do not account for even half of the observed (α,pn) radiochemically determined cross sections at these bombardment energies. It is certainly to be expected that reactions involving the emission of a proton and neutron would contribute to this reaction. It is not clear in this case, however, just what range of proton energies toassociate with the (α,pn) reaction. As some of the previously discussed radiochemical work indicates a large contribution to this reaction from direct-interaction processes, a crude analysis based on this assumption is possible. Prompt emission of a low-energy nucleon by direct process, leaving the nucleus highly excited, would on the average lead to multiparticle evaporation. A prompt particle, leaving the nucleus excited to less than the binding energy of two nucleons, might be expected to contribute considerably to the (α,pn) reaction. When the residual excitation energy of the nucleus is only of the order of the binding energy of two nucleons, neutron evaporation should be considerably favored over proton evaporation, at least in the medium and heavy elements, because of the Coulomb barrier effect on the charged particle. Emission of the proton as a prompt high-energy particle, leaving the nucleus just sufficiently

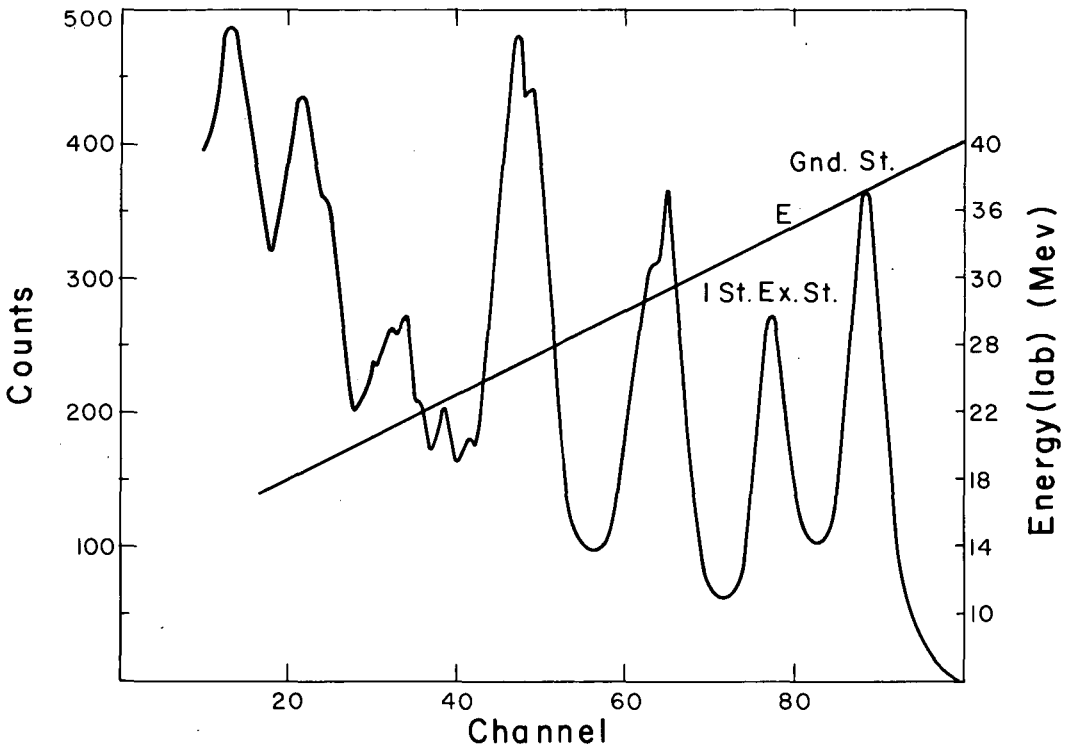

MU-16958

Fig. 7-a. Deuteron energy spectrum obtained at 15 degrees (lab) for the $Be^9(\alpha,d)B^{11}$ reaction. The helium ion energy was 48-Mev. Plotted are the relative number of counts and energy versus the pulse-height analyzer channel number. The curve labeled E corresponds to the energy scale.

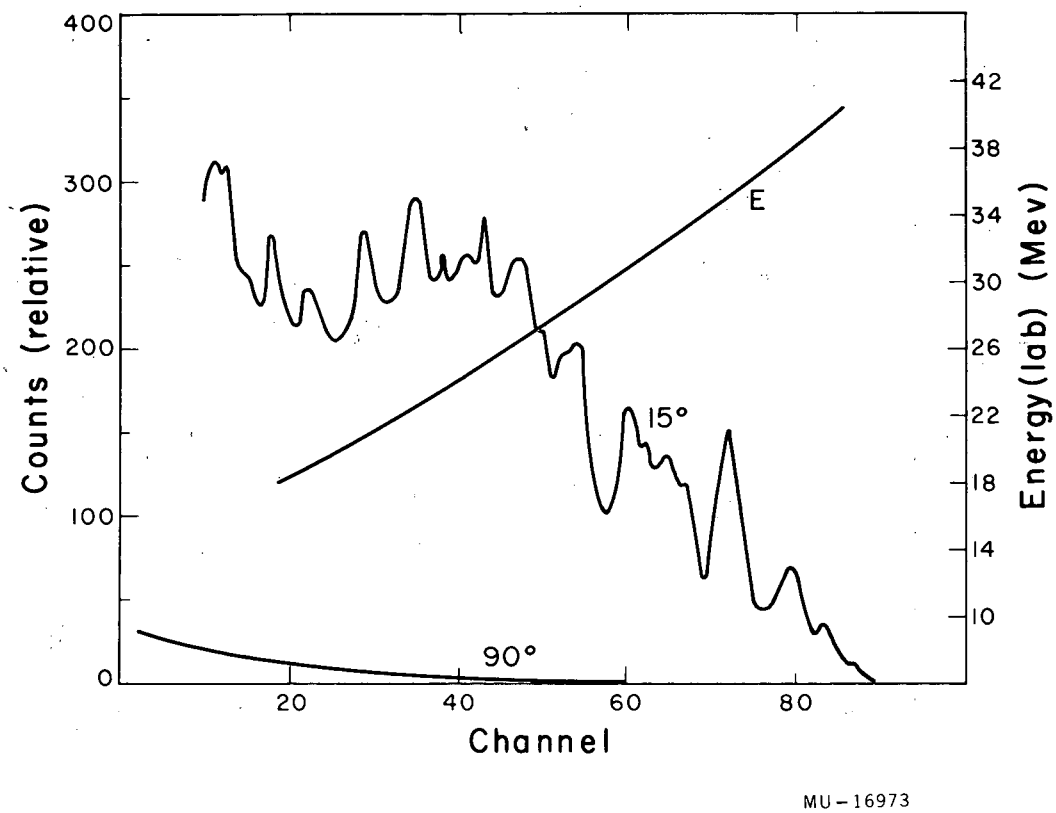

Fig. 7-b. Deuteron energy spectrum obtained at 15 and 90 degrees (lab) for the $Al^{27}(\alpha,d)Si^{29}$ reaction. The helium ion energy was 48-Mev. Plotted are the relative number of counts and energy versus the pulse-height analyzer channel number. The curve labeled E corresponds to the energy scale.

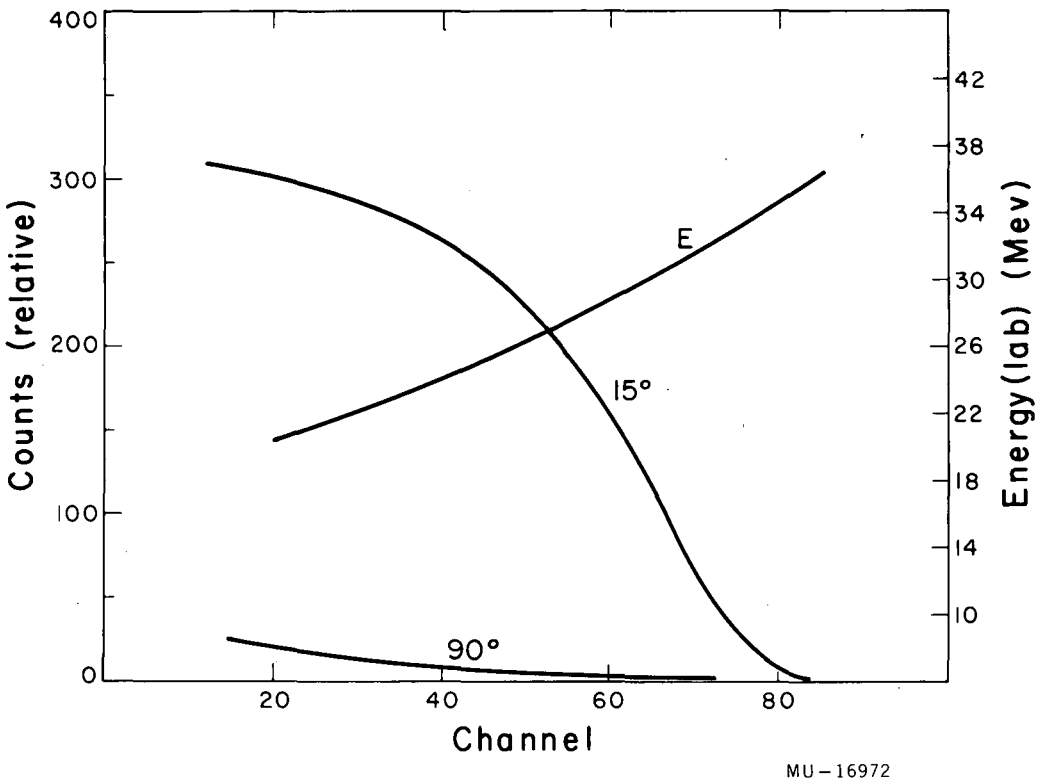

Fig. 7-c. Deuteron energy spectrum obtained at 15 and 90 degrees (lab) for the $Pd^{110}(\alpha,d)Ag^{112}$ reaction. The helium ion energy was 48-Mev. Plotted are the relative number of counts and energy versus the pulse-height analyzer channel number. The curve labeled E corresponds to the energy scale.

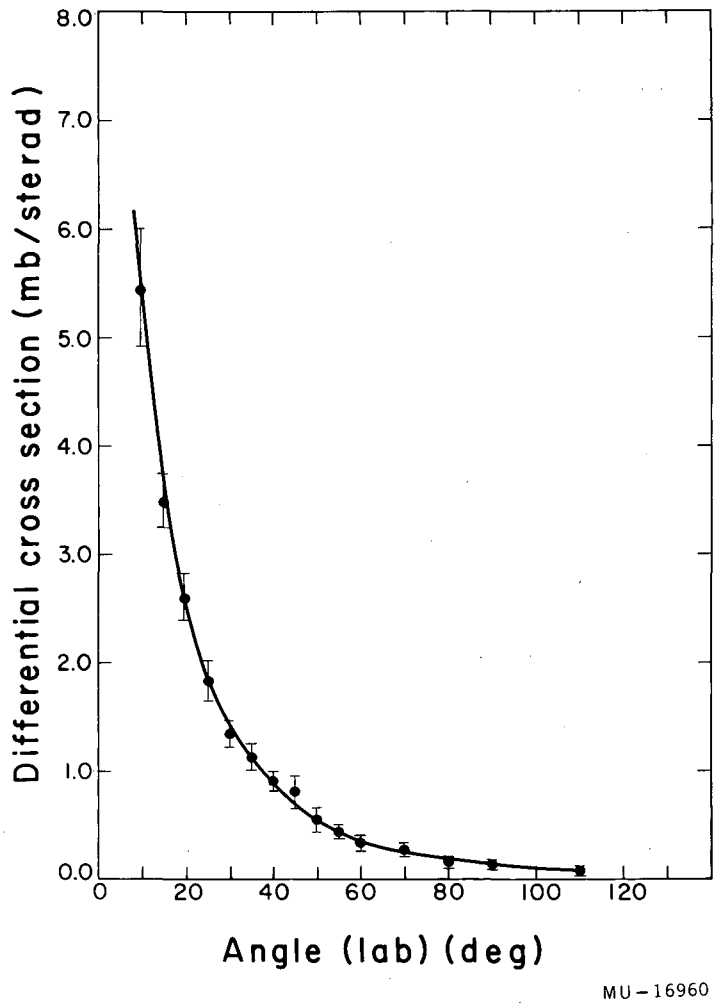

Fig. 8-a. Angular distribution of deuterons associated with the (α,d) reaction of Al^{27} with 48-Mev helium ions.

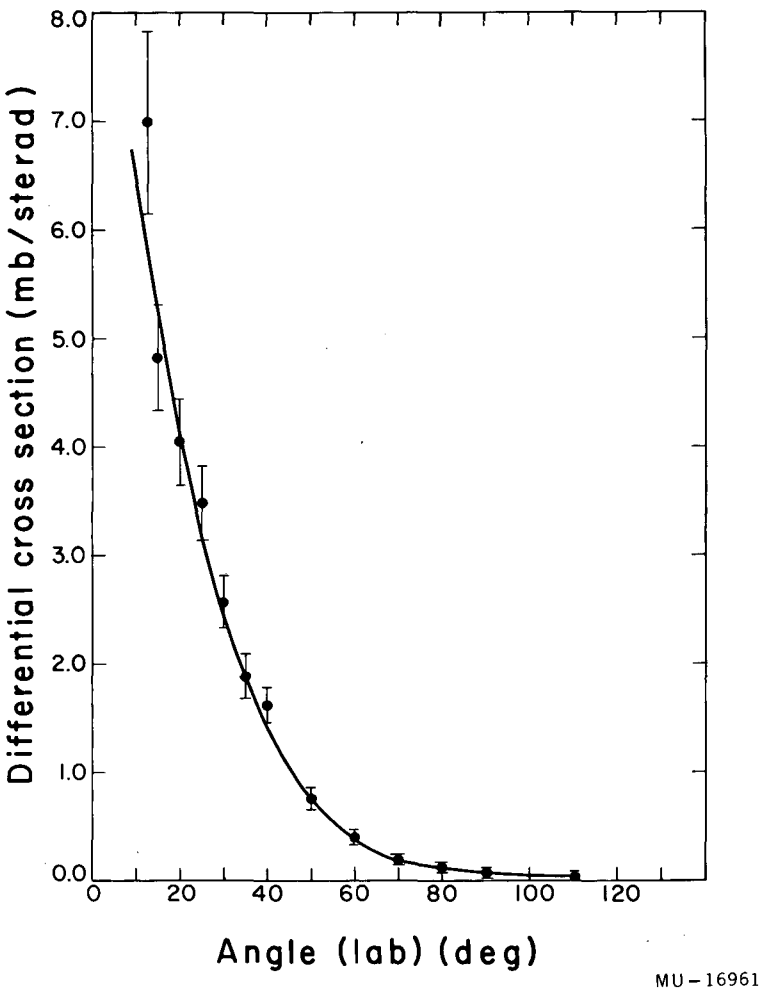

Fig. 8-b. Angular distribution of deuterons associated with the (α,d) reaction of Pd^{110} with 48-Mev helium ions.

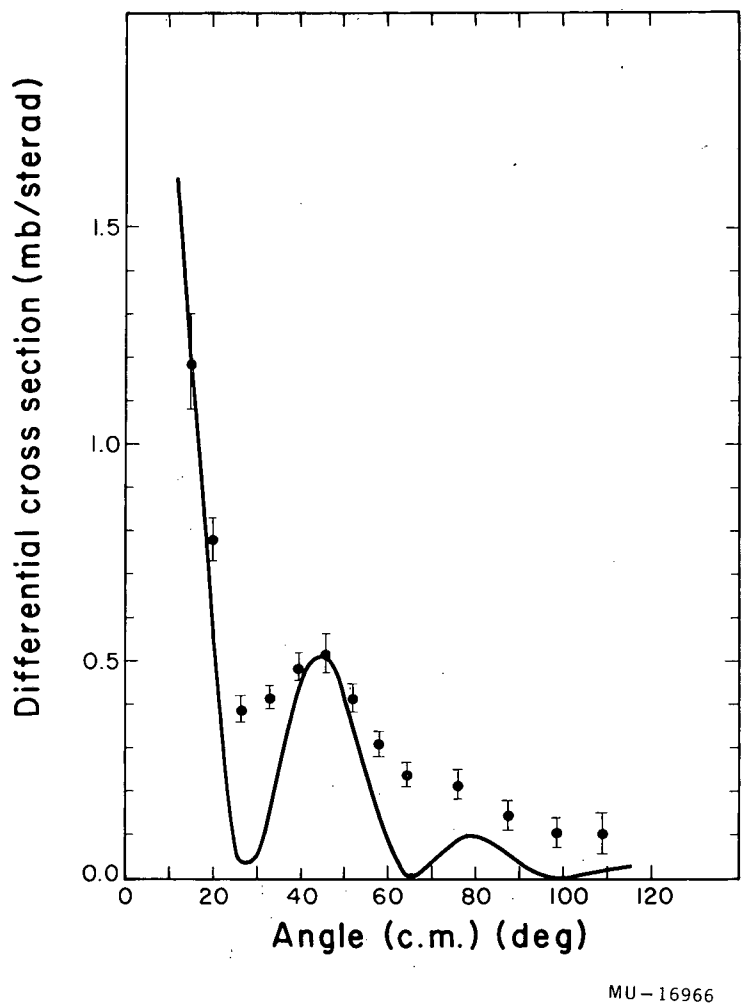

Fig. 9-a. Angular distribution of deuterons from the $Be^9(\alpha,d)B^{11}$ reaction leading to the ground state of B^{11} ($\ell = 2$). The points represent the experimental data. The solid line is a theoretical curve calculated according to Butler's theory with $r_o = 5.7 \times 10^{-13}$ cm.

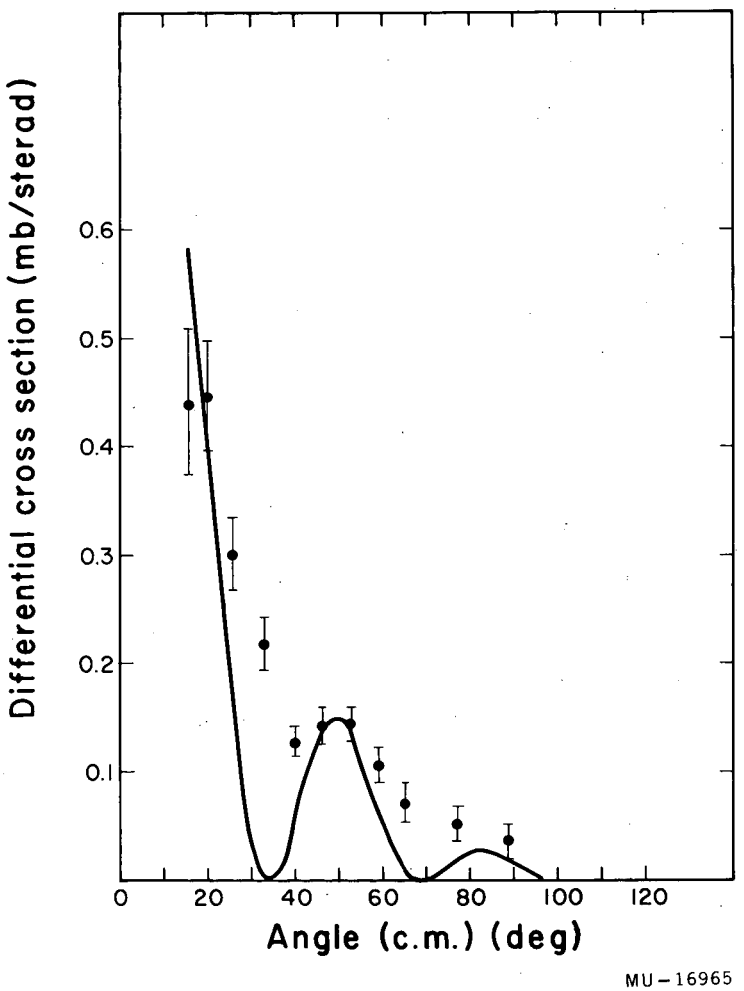

Fig. 9-b. Angular distribution of deuterons from the $Be^9(\alpha,d)B^{11}$ reaction leading to the first excited state of B^{11} ($\ell = 0$). The points represent the experimental data. The solid line is a theoretical curve calculated according to Butler's theory with $r_o = 5.7 \times 10^{-13}$ cm.

excited to evaporate a neutron, would seem to be a reasonable direct process involving proton emission. This picture is obviously too simplified, as it neglects the possibility of the simultaneous emission of a neutron and a proton of medium energy.

The assumption was made that, from the entire energy spectrum, only those protons contributed to the (α,pn) reaction whose observed energies corresponded to a residual nucleus left with just sufficient energy to evaporate only one neutron. Protons were accepted as soon as their energy corresponded to leaving the residual nucleus excited to an energy that was the sum of the binding energy of one neutron plus its average evaporation energy plus the binding energy of a second neutron. The average evaporation energy of the first neutron was taken as 2T, computed from Lang's and Le Couteur's empirical formula[46]

$$T = \sqrt{\frac{10.5\ E}{A}},$$

where T is the nuclear temperature, A is the mass number, and E is the excitation of the residual nucleus. As the average evaporation energy was of interest for those cases in which the residual nucleus was left excited to the binding energy of the second neutron, E was taken as $Q_{\alpha,pn} - Q_{\alpha,p2n}$. The acceptable energy range for protons was taken as $E_\alpha + Q_{\alpha,pn} > E_p > E_\alpha + Q_{\alpha,p2n} - 2T$. An error of 1 Mev in the estimated energy corresponds to about a 5% error in the total integrated cross section.

It has been assumed in this analysis that only a small contribution to the proton spectra used for the cross-section calculations results from processes involving the re-emission of the incident helium ion after proton emission, i.e., the $(\alpha,\alpha'p)$ reaction. Protons in the energy range used in the calculations could be obtained from events in which the helium ion was re-emitted with an energy getween about 5 and 15 Mev. The work of Igo[47] and the work of Merkle,[48] dealing with inelastic scattering of helium ions of about 40 Mev show that helium ions re.emitted with energies in the range of 5 to 15 Mev tend to have angular distributions symmetric about 90° and nearly isotropic, as one

would expect from an evaporation process. As the Coulomb barrier discriminates against charged-particle evaporation, one would expect neutron evaporation to be more probable in most cases than helium-ion evaporation.

It has been noted[5] that the $(\alpha,\alpha'n)$ reaction is a fairly prominent one, and this reaction has a cross section of about 40 to 50 mb in the bombardment of U^{238} with helium ions. The $(\alpha,\alpha'p)$ reaction of Pu^{239} has been shown to be < 1 mb.[49] These facts would suggest that the $(\alpha,\alpha'x)$ reaction, where x is a neutron or proton, proceeds mainly by the inelastic scattering of the incident helium ion with high energy leaving the excited target nucleus to de-excite by the evaporation of a low-energy nucleon, primarily a neutron.[5]

5. Proton Cross Sections

The angular distributions of protons corresponding to the (α,pn) reaction, as defined, were obtained from the entire energy spectrum by selection of protons of the proper energy range. The differential cross sections and the total integrated cross sections for the elements studied are listed in Table II. Included are the differential cross sections leading to the 1.67- and 3.76-Mev level of B^{12} obtained in the helium-ion bombardment of Be^9. Figure 10 shows some typical proton spectra obtained for beryllium, aluminum, and bismuth. Figure 11 shows plots of the variation of the differential cross sections with angle for the production of protons leading to the (α,pn) reaction on aluminum and bismuth. The other elements studied give similar results. Figure 12 shows the angular distributions of protons leading to the 1.67- and 3.76-Mev levels of B^{12}, together with theoretical curves calculated by using Butler's theory.

Errors in the values of the proton angular distribution cross sections were nearly constant with angle, and arose primarily from uncertainties in target thicknesses and energy calibrations. Errors due to counting statistics were usually quite low. The estimated limits of error are 10 to 15%. Errors listed for Be^9 are relative errors estimated from resolution of energy-spectra peaks and counting statistics. The low-lying levels of B^{12} lay relatively close together. With the equipment used, it was difficult to resolve the peaks in the proton spectra

Table II

Proton differential cross sections as a function of laboratory-system angle for bombardment with helium ions at 41 and 48 Mev (millibarns/steradian)

Angle (lab system) (degrees)	Isotope											
	Al^{27}		Ni^{60}		Pd^{110}		Bi^{209}		U^{238}		Be^{9}	
	41 Mev	48 Mev	41 Mev	48 Mev	41 Mev	48 Mev	41 Mev	48 Mev	41 Mev	48 Mev	48 Mev 1.67 Mev state	48 Mev 3.76 Mev state
12.5	15.0			46.3		23.1		8.87				0.226±0.036
15	16.8	18.7	47.2	40.4	20.2	20.9	7.14	7.16	5.56	6.25	<0.025	0.130±0.020
20	13.8	14.8	34.9	32.8	16.7	16.9	6.20	6.59	4.26	4.47	<0.051	0.065±0.016
25	11.0	12.1	25.7	25.6	13.7	12.5	5.59	5.27	3.56	3.41	0.062±0.018	0.026±0.013
30	8.07	10.7	19.0	21.4	9.43	8.79	4.15	4.52	2.90	3.02	0.086±0.017	<0.065
35			17.3		7.31	6.72					0.018±0.0092	0.065±0.045
40	5.56	7.92	14.7	16.1	5.15	5.08	2.95	3.28	1.88	2.35	0.070±0.014	0.131±0.059
50	4.38	4.89	8.38	10.3	3.71	3.33	2.12	2.16	1.20	1.23	0.018±0.007	0.036±0.011
60	2.74	3.82	6.13	7.02	2.72	2.18	1.42	1.50	1.02	0.88	0.002±0.001	0.033±0.010
70		3.00	4.91	3.79	1.45	1.36		0.92		0.55	0.005±0.003	0.022±0.007
80	1.60	2.26	3.85	2.64	0.93	0.85	0.78	0.59	0.56	0.31	0.006±0.003	0.005±0.003
100	1.26	1.29	1.94	1.23	0.50	0.43	0.38	0.30	0.25	0.19		
120	0.86	0.79	1.60			0.31				0.06		
150				1.22		0.14		0.20				
Total cross section (mb)	34.2	40.8	81.4	76.3	30.5	28.9	15.8	15.7	10.8	10.1		

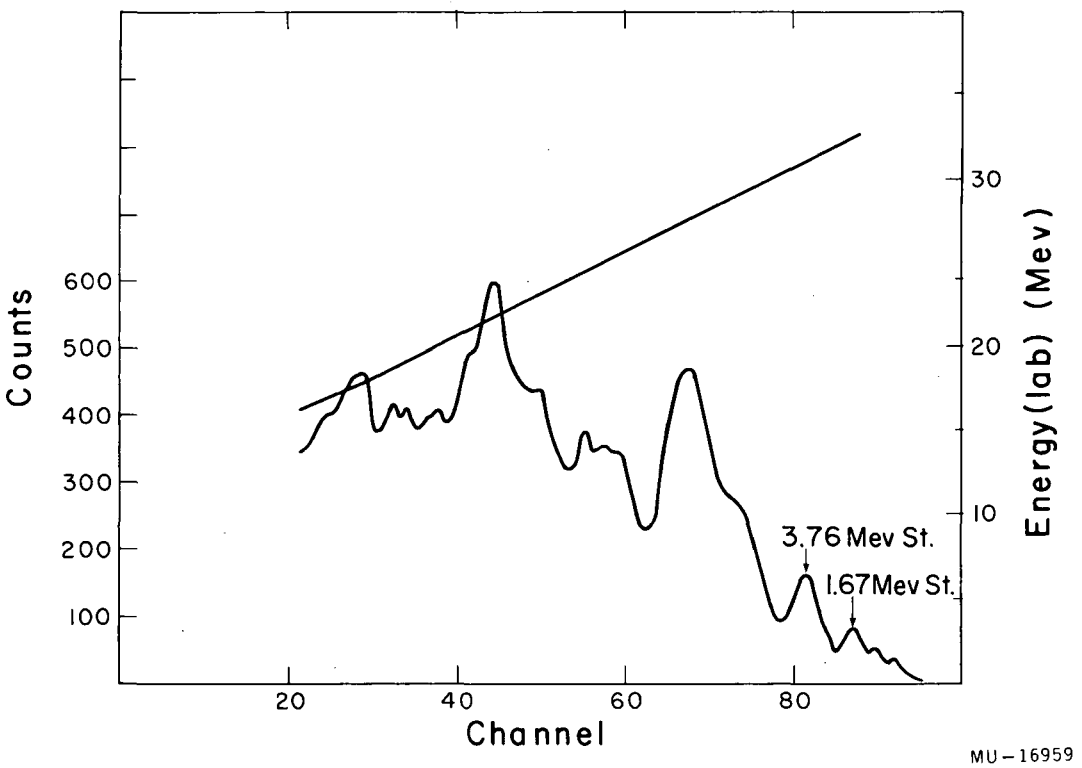

Fig. 10-a. Proton energy spectrum obtained at 15 degrees (lab) for the $Be^9(\alpha,p)B^{12}$ reaction. The helium ion energy was 48 Mev. Plotted are the relative number of counts and energy versus the pulse-height analyzer channel number. The curve labeled E corresponds to the energy scale.

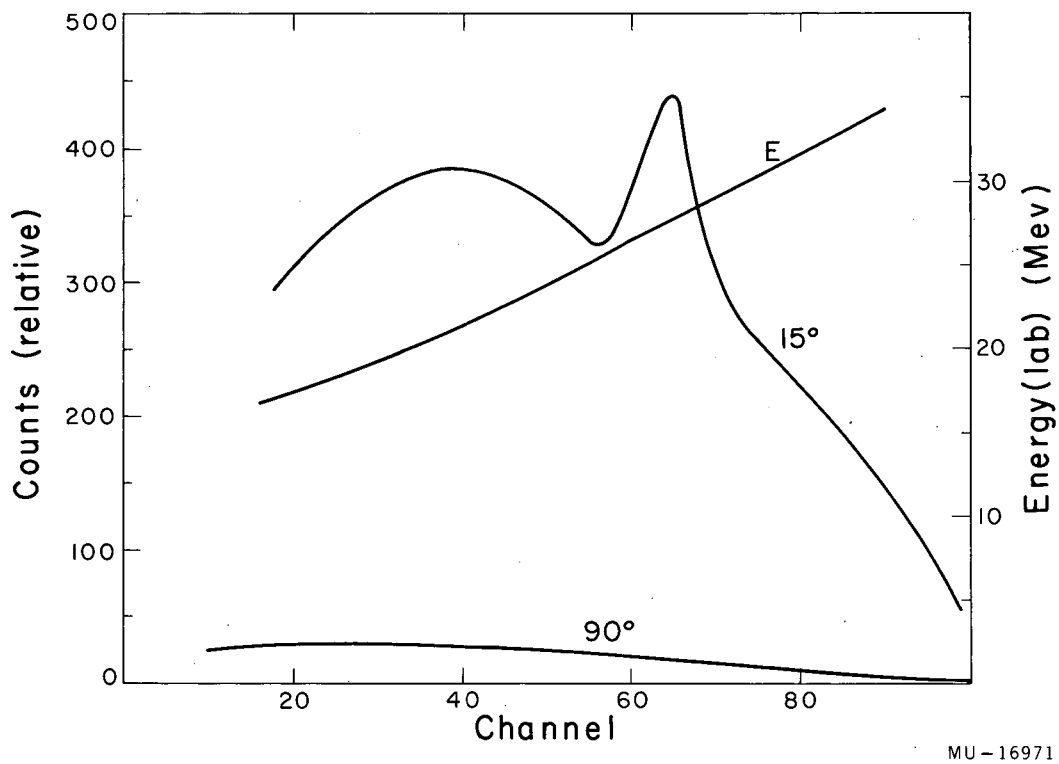

Fig. 10-b. Proton energy spectrum obtained at 15 and 90 degrees (lab) for the $Al^{27}(\alpha,p)Si^{30}$ reaction. The helium ion energy was 48 Mev. Plotted are the relative number of counts and energy versus the pulse-height analyzer channel number. The curve labeled E corresponds to the energy scale.

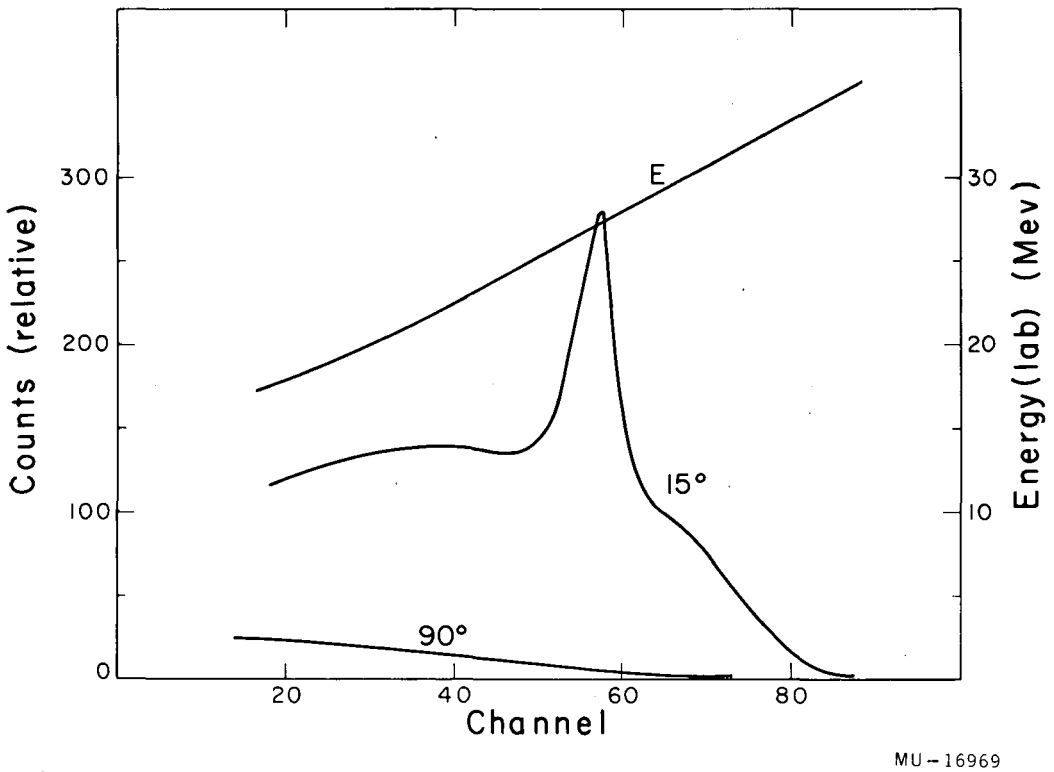

Fig. 10-c. Proton energy spectrum obtained at 15 and 90 degrees (lab) for the $Bi^{209}(\alpha,p)Po^{212}$ reaction. The helium ion energy was 48 Mev. Plotted are the relative number of counts and energy versus the pulse-height analyzer channel number. The curve labeled E corresponds to the energy scale.

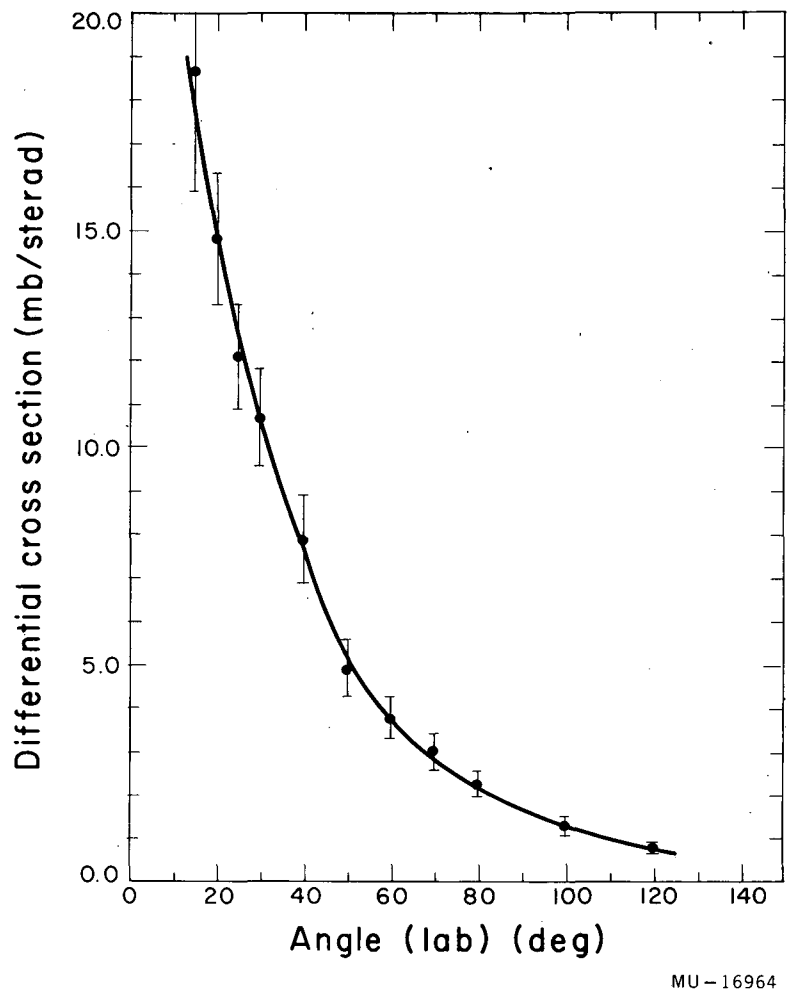

Fig. 11-a. Angular distribution of protons assumed to be associated with the (α,pn) reaction of Al^{27} with 48-Mev helium ions.

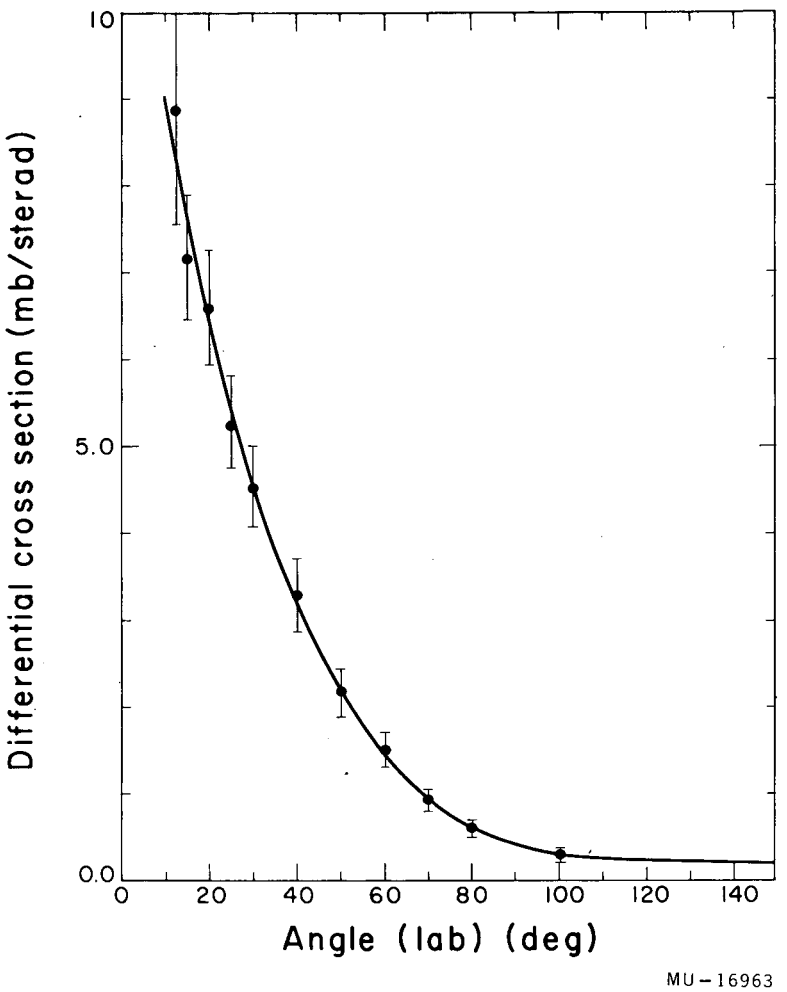

Fig. 11-b. Angular distribution of protons assumed to be associated with the (α,pn) reaction of Pd^{110} with 48-Mev helium ions.

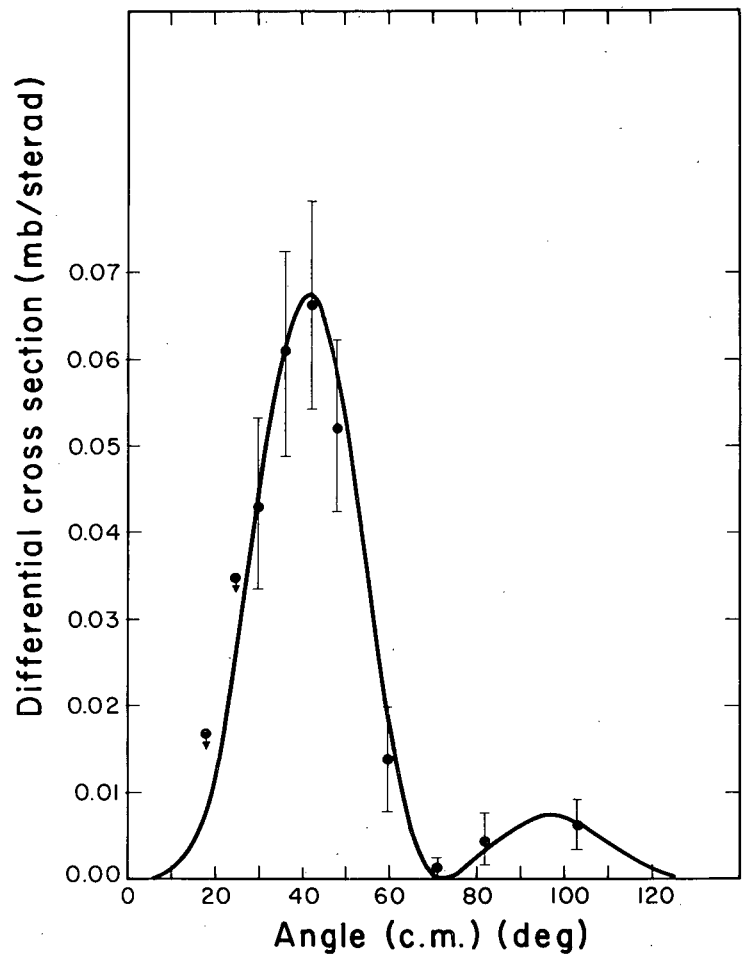

MU-16967

Fig. 12-a. Angular distribution of protons from the $Be^9(\alpha,p)B^{11}$ reaction leading to the 1.67-Mev state of B^{11} ($\ell = 0$). The points represent the experimental data. The solid line is a theoretical curve calculated according to Butler's theory with $r_o = 5.7 \times 10^{-13}$ cm.

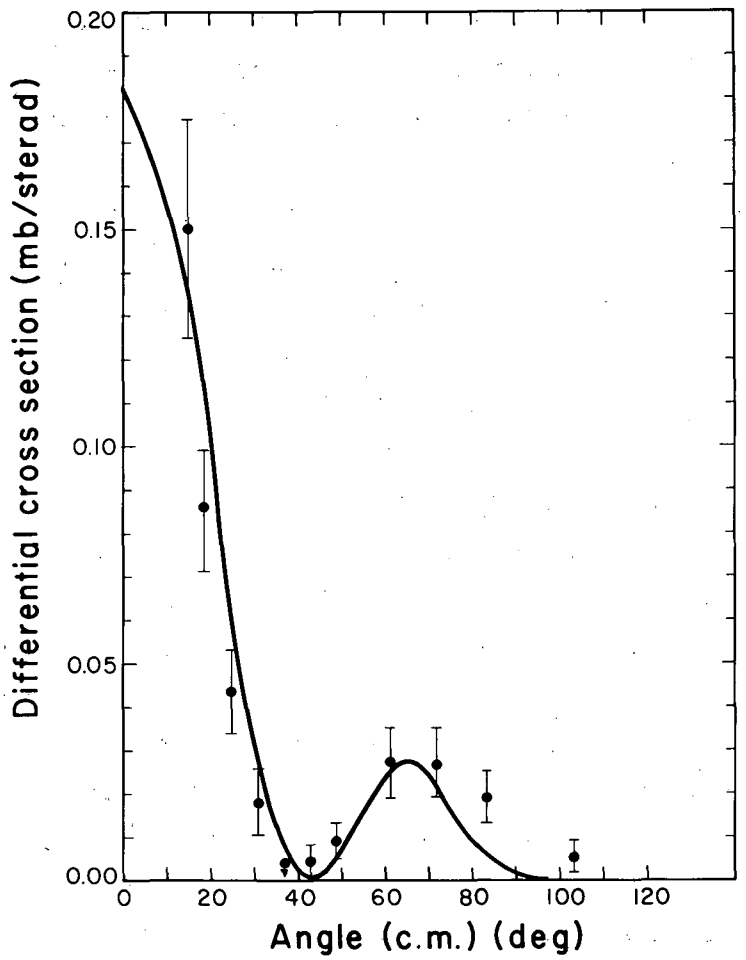

MU-16968

Fig. 12-b. Angular distribution of protons from the $Be^9(\alpha,p)B^{11}$ reaction leading to the 3.76-Mev state of B^{11} ($\ell = 1$). The points represent the experimental data. The solid line is a theoretical curve calculated according to Butler's theory with $r_o = 5.7 \times 10^{-13}$ cm.

corresponding to transitions to these levels; consequently the differential cross sections obtained are only approximate, and their absolute magnitude may be considerably in error. They were obtained primarily to compare with a Butler-theory calculation.

If the (α,pn) reaction on a uranium target proceeds by the evaporation of a neutron after prompt proton emission, fission occurs in competition with the neutron evaporation. The (α,pn) cross sections calculated from the scattering-chamber data are therefore too large. One may estimate a correction to the scattering data by decreasing the calculated cross sections in the ratio of the neutron-emission width to neutron-emission-plus-fission width, $\Gamma_n/(\Gamma_n + \Gamma_f)$, of the nucleus undergoing competition, i.e., Np^{241}. The value of $\Gamma_n/(\Gamma_n + \Gamma_f)$ for Np^{241} can be estimated from curves by Vandenbosch and Huizenga,[50] and was taken as 0.57.

6. Proton Spectra Contamination

A sharp maximum occurred in the proton-energy spectra at forward angles for all elements studied. This peak showed a marked downward shift in energy as the angle of observation was increased, and disappeared from the observable energy range at an angle of about 45°. The energy of this peak had the same angular dependence for all the elements. The dependence on energy and angle fitted quite well with that calculated for the interaction of helium ions with free hydrogen nuclei. The full width at half maximum of this peak was 8 to 12%, which is slightly slightly larger than for a peak corresponding to a group of particles of discrete energy. If this peak corresponded to protons being "knocked out" of the nucleus by an incident helium ion, one would expect a smearing out of the otherwise unique correlation between the angle and energy of the emerging particle due to the momentum distribution of the nucleons in a nucleus. Certain investigations[51,52,53] indicate that the momentum distribution should produce a proton peak whose full width at half maximum would be 10 to 20 Mev, rather than the 2 to 3 Mev observed. This observed peak

is attributed to the interaction of the bombarding helium ions with hydrogenous material on the surfaces of the targets (possibly a thin oil film). This phenomenon has also been observed by others.[54] The peak was consequently subtracted out of the energy spectra.

IV. DISCUSSION

A. Angular Distributions, Energy Spectra, and Cross Sections Expected from Statistical-Model and Optical-Model Interactions

Deuterons and protons produced in reactions proceeding via formation of a compound nucleus and statistical decay should exhibit certain characteristic features in their energy and angular distributions. In low nuclear excitation in the light elements, in which the level densities are low, it is possible to obtain groups of particles of discrete energies corresponding to decay involving separate levels.[55,56]

In medium and heavy elements, at energies corresponding to excitation of the nucleus to its continuum, the energy spectrum to be expected from the statistical decay of compound nuclei has been given by Weisskopf.[57] With the introduction of the idea of nuclear temperature and entropy, the equation giving the energy spectra to be expected can be written in its simplest form

$$P_j\,(E)\,dE = \text{const}\ \sigma\,(E)\,E\,\exp\,(-E/T)\,d\,E,$$

where $P_j\,(E)\,dE$ = the probability per unit time for the emission of the particle j with energy between E and E + dE,

$\sigma\,(E)$ = cross section for the capture of the particle j by the target nucleus,

E = energy of emitted particle,

T = nuclear temperature.

If the variation of $\sigma\,(E)$ with E is neglected, one obtains the familiar Maxwellian distribution in the energy of the emitted particles, with the most probable energy occurring at E = T. If the particles are charged, the probability for emission is quite energy-sensitive; low values of E mean that the probability for penetration of the barrier is low and $\sigma\,(E)$ distorts the Maxwellian distribution by shifting the maximum to higher energies.[57] The most probable energy is slightly above that corresponding to the Coulomb barrier.

The statistical theory assumes that the compound nucleus has lost all memory of its mode of formation by the time the particle is emitted. It might be expected that the angular distribution of decay products should be isotropic in the center-of-mass system. This point has been examined by Wolfenstein[58] and further developed by Hauser and Feshback.[59] If all the assumptions[58] of statistical decay are met, so that certain simplifications can be made, the angular part of the calculated differential cross section can be expressed as a function of $\cos^2 \theta$; θ is the angle of the emitted particle relative to the incident particle. It appears that the angular distribution of the product particles need not be isotropic, but must be symmetric about a plane at 90°.

The cross section for the production of charged particles should show a strong z dependence. In order to be emitted with appreciable probability, the escaping particles must have kinetic energy exceeding the Coulomb-barrier energy. On the statistical model, the average kinetic energy of the emitted particles is of the order of 2T. For heavy elements, $T \simeq 1$ Mev and the barrier for protons > 10 Mev, so that $T \ll$ barrier. The relative width for charged-particle emission (Γ_c/Γ_{total}) should decrease rather rapidly with z. Figure 13 is a plot of Γ_c/Γ_{total} calculated for proton and deuteron emission from nuclei excited to 40 Mev as a function of A. The calculation was made for the most stable even-even nuclei of a given A, using the equations given by Dostrofsky and co-workers[60] Here Γ_{total} is the sum of the calculated widths for emission of neutrons, protons, deuterons, tritons, and alpha particles. These widths can shift up or down by a factor of about 2 for other nuclear types because of the differences in level densities.

The optical-model effects on the energy distribution of reaction components are rather varied. There has been little work done on the product particles resulting from helium-ion bombardments leading to other than single levels, except to show that the cross sections for the production of high-energy charged particles are greater than expected from statistical theory.[9,10] Inelastically scattered protons, neutrons, and

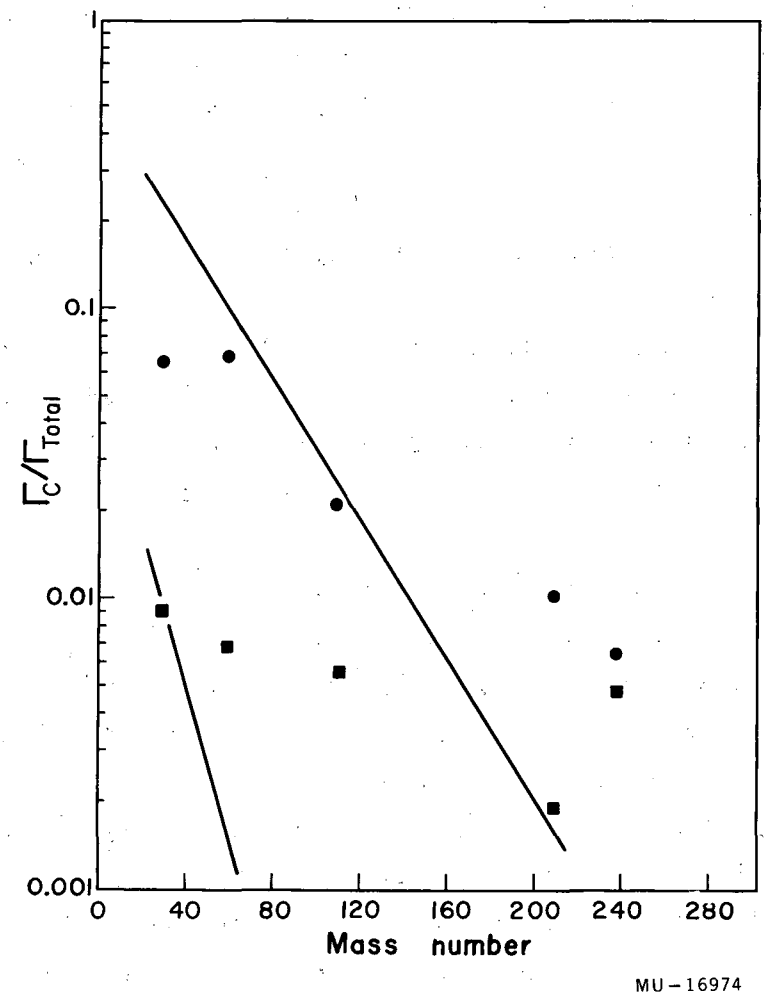

Fig. 13. A plot of the relative widths for proton and deuteron emission, Γ_c/Γ_{total}, versus mass number for the most stable even-even nuclide of a given mass number excited to 40 Mev. The circles are the experimentally determined widths, σ_c/σ_{total}, for protons associated with the $(\alpha,pn$ reaction of Al^{27}, Ni^{60}, Pd^{110}, Bi^{209}, and U^{238}. The squares represent σ_c/σ_{total} for deuterons.

helium ions show rather broad peaks in their energy spectra.[9,61] Direct interactions seem to show this characteristic flat high-energy distribution of product particles. This leads to a higher average emission energy than that of the decay particles of the compound nucleus.[9] This is because surface interactions contribute a great deal and involve only a few nucleons, which tends to lead to large transfers of energy to the emitted particles.

The optical components always tend to give angular distributions peaked in the forward direction,[62,63,64] especially at high energies. Since only a few target nucleons at most are involved in a direct reaction, the forward momentum of the incident particle causes forward peaking of the reaction products. Forward asymmetric peaking about 90° is taken as evidence for a direct-interaction process.[9] For reactions of helium ions with nuclei in which particles of discrete energies are emitted -- corresponding to interactions involving separate levels -- Butler's theory has been quite successful in predicting the variation of differential cross sections for these particles with center-of-mass angle.[7,11,65,66]

Considerable experimental data[9] have shown that direct-interaction processes generally yield charged particles with energies $E \gtrsim$ Coulomb barrier, and do not exhibit the strong Z dependence of compound-nucleus reactions. Thus, a yield of charged particles substantially in excess of that predicted by the statistical model is evidence for direct-interaction processes.

B. Butler's Theory

Butler's theory[62,67] was originally derived for deuteron stripping reactions; however, it was soon shown[7,45,64,68] that the angular distributions from other types of surface reactions should be very similar and be similarly dependent on spin and parity changes between the initial and final nuclear states.

A simple form of Butler's theory can be written as

$$\frac{d\sigma}{d\Omega} = A|F|^2 \, |j_{(\ell)} \, (q\, r_o)|^2 ,$$

where $\frac{d\sigma}{d\Omega}$ is the differential cross section per unit solid angle; A is taken as a constant for a given reaction energy (it involves level widths, factors of the wave functions involved, and assorted constants); F is called a form factor and is a decreasing function with increasing angle; $j_{(\ell)}(q\, r_o)$ is a spherical Bessel function of order ℓ, where ℓ is the relative change in angular momentum between the initial and final nuclei; q is the absolute value of the vector difference between the vector wave numbers of the bombarding particle ($\vec{k}_i$) and final light product particle ($\vec{k}_f$); after correction for the finite masses of the initial and final nuclei (M_i, M_f), q is given by $|\vec{k}_i - \frac{M_i}{M_f}\vec{k}_f|$; r_o is the radius of interaction. The A and r_o are usually taken as adjustable parameters; r_o has the property of shifting the peaks in the angular distribution, and A adjusts the absolute magnitude of the cross section.

The value of ℓ is determined by conservation of angular momentum according to the equation

$$|\vec{J}_i + \vec{J}_f + \vec{i}|_{min} \leq \ell \leq J_i + J_f + i \,.$$

where $\vec{J}_i$ and $\vec{J}_f$ are the spins of the initial target nucleus and final residual nucleus, respectively; $\vec{i}$ is the vector sum of incident and escaping particles. Parity must be conserved in the choice of ℓ. When several values are allowed, the lowest ℓ is taken as contributing the most to the reaction.

The form factor is made up of the internal wave function of the incoming particle and the wave function of the incoming particle expressed as a plane wave. It is a decreasing function with increasing momentum change between the incoming and outgoing particles, i.e., with increasing angle. It represents the fact that the incident particle always prefers to split in such a way that the direction of the outgoing particle is as close as possible to the direction of motion of the incident particle.

The approximations used in the derivation of Butler's expression have been discussed elsewhere.[45]

C. Angular Distribution From $Be^9(\alpha,d)B^{11}$ and $Be^9(\alpha,p)B^{12}$ Reactions

Butler's theory has predicted, with fair success, the angular distribution of protons[66,69,70] and tritons[11] produced in helium-ion bombardment of some light elements. It would be of interest to make a trial at fitting the angular distributions of deuterons from the (α,d) reaction on Be^9, in addition to the protons from the (α,p) reaction.

The angular distributions of the deuterons leading to the ground and first excited states of B^{11} and of the protons leading to the 1.76-Mev and 3.76-Mev states of B^{12}, shown in Figs. 9 and 12, agree fairly well with those predicted by Butler's theory. This clearly shows their origin from direct-interaction processes.

It was not possible to use a rigorous theoretical form factor, as this requires a knowledge of the wave function of helium. Hunting and Wall have shown that the approximate form factor given by Butler does not appear to contribute enough to forward peaking of the reaction products in helium-ion interactions.[66] They find that a factor of the form

$$\exp\left[- (k_i - k_f)/Q_o^{\,2} \right] ,$$

where $Q_o^{\,2}$ is an adjustable parameter, gives a better fit to the data. This factor gives more emphasis to forward peaking than Butler's factor.

The best fit of the experimental data seems to be obtained by using an interaction radius of 4.7×10^{-13} centimeter. This value is slightly larger than the 4.3×10^{-13} cm contact distance obtained from the sum of the radius of Be^9, as calculated from the expression $r = 1.5 \times 10^{-13} A^{1/3}$ cm, and the radius taken for the helium ion, 1.2×10^{-13} cm.

The ℓ values chosen for the spherical Bessel functions were 2 and 0 for the ground-state ($J = 3/2-$) and first-excited-state ($J = 1/2-$) transitions to B^{11}, and 0 and 1 for the 1.67-Mev-state ($J = 1-, 2-$) and the 3.76-Mev-state ($J = 2+$) transitions to B^{12}. The ground-state spin of Be^9 was taken as $3/2-$. All the spins were taken from the compilation by Ajzenberg and Lauritsen.[42]

After consideration of the details of the reaction, an ℓ value of 2 was taken for the reaction of $Be^9(\alpha,d)B^{11}$ ground-state transition, rather than the allowed ℓ value of 0. If one considers the incoming helium ions, spin 0+, breaking up and producing a deuteron, spin 1+, as an outgoing particle, then the proton and neutron that enter the nucleus very likely have their spins of 1/2+ aligned to give a resultant spin of 1+. (This assumes no spin flip.)

A consideration of the shell-model structure of Be^9 shows that, to lead to a ground-state transition, both the proton and neutron must go into a $p_{3/2}$ state. Each must have one unit of orbital angular momentum added onto the intrinsic spins of 1/2 to give a resultant J value of 3/2; $J = \ell + S$. As their intrinsic spins are aligned parallel, then their angular-momentum vectors must also be aligned parallel. This results in a change in angular momentum of 2 rather than 0. In order to fit the experimental data to an ℓ value of 0, the very small value of $r_o = 3.2 \times 10^{-13}$ cm must be used; the data are fitted well with an ℓ of 2 and the much more reasonable radius of 4.7×10^{-13} cm.

Butler has pointed out that, as the helium ion cannot be considered loosely bound, some of the nuclear approximations are not valid.[45] Also, for the doubly charged helium ion, the Coulomb effects are rather large. These factors tend to fill in the valleys between the peaks of the theoretical distributions and tend to broaden and shift the peaks. The cross sections at large angles are larger than the theory would predict. This seems to be a general failing of the theory; factors leading to this have been discussed elsewhere.[71]

D. Energy Spectra and Angular Distributions of Protons and Deuterons Involving Transitions to Many Levels

In light elements, such as beryllium and aluminum, transitions to well-separated nuclear energy levels near the ground state give rise to protons and deuterons of discrete energies. As the nuclear excitation and the atomic number increase, the density of nuclear levels increases and the average level spacing decreases. Using apparatus of moderate

resolving power, one expects proton and deuteron energy spactra involving states of high nuclear excitation, and those associated with heavy elements to consist entirely of continuous spectra.

The proton and deuteron spectra obtained for aluminum and heavier elements were for the most part continuous, and exhibited the broad distributions, with large contributions from particles of high energy, characteristic of the optical-model component of nuclear reactions. Except at angles greater than 90°, they are very different from the type of exponential distribution characteristic of evaporation from an excited compound nucleus.

The angular distributions of protons and deuterons corresponding to the (α,d) and (α,pn) reactions, as defined, show very strong forward peaking with little contribution to the integrated cross sections from angles greater than 90°. This forward peaking is associated with particles of the entire observed energy spectrum and is not limited to just the energy range taken for the calculation of the integrated cross sections.

The cross sections for the production of deuterons and protons obtained from the scattering-chamber experiments are considerably larger than one would expect from statistical-model calculations. Even though they represent only 10 to 20% of the total proton and deuteron energy spectra, the cross sections for the production of protons and deuterons taken as contributing to just the (α,pn) and (α,d) reactions are as large as or larger than one would predict for the total proton and deuteron evaporation probabilities for nuclei excited to 40 Mev. Figure 13 is a comparison of calculated relative widths for proton and deuteron emission from nuclei excited to 40 Mev with the experimentally determined relative widths for emission of protons and deuterons corresponding to just the (α,pn) and (α,d) reaction. The experimental relative widths were taken as the ratio of the experimental cross section to the geometric cross section, σ_c/σ_{total}; the observed widths for the emission of protons and deuterons range from one to several orders of magnitude times as large as the statistical model would predict as one proceeds from light elements ($A \sim 27$) to heavy elements ($A \sim 200$).

The three pieces of information obtained -- i.e., the energy distributions, the angular distributions, and the total cross sections -- point to the conclusion that the processes yielding protons and deuterons associated with the (α,pn) and (α,d) reactions of nuclei with helium ions, in the energy range 40 to 48 Mev, are related to optical-model interactions and have little to do with compound-nucleus formation.

E. Discussion of Radiochemically Determined Cross Sections and Comparison With Scattering-Chamber Cross Sections

The radiochemical excitation functions for the (α,pn) reaction exhibit several distinguishing features. In the region of Ni^{60}, Ni^{61}, and Fe^{54}, a large maximum of several hundred millibarns occurs in the excitation functions at a helium-ion bombarding energy of about 30 Mev. As the helium-ion energy is increased, the magnitude of the cross section decreases rapidly at first, but then appears to "tail out" and decrease more slowly with energy.

As one proceeds to slightly heavier nuclides, such as Se^{80} and Pd^{110}, the observed magnitudes of the (α,pn) cross sections show a drastic reduction (factor of ~10) over that in the nickel region. The cross section decreases more slowly (factor of ~3) with Z as one proceeds from Pd^{110} to the region of Pu^{238}. For Pd^{110} and the heavier elements studied, the excitation functions tend to show a broad maximum at a constant helium-ion energy of about 40 Mev.

As others have pointed out,[5,6] the (α,pn) cross sections are as large as the corresponding (α,2n) cross sections in the heavy-element region where fission also can be induced with helium ions of the energies used here; (α,2n) cross sections are much larger in nonfissioning heavy elements such as lead and bismuth.[72,73] Also, only a small decrease in the magnitude of the (α,pn) cross section occurs as one proceeds from the nonfission region -- i.e., lead and bismuth -- to the fission region; a large decrease is observed in the magnitude of the (α,2n) reaction.

Some of the features observed can be explained by the scattering-chamber data, others can not. Table III compares the cross sections for

Table III

Comparison of cross sections for (α,pn) reactions obtained from radiochemical and scattering-chamber data from bombardment of various isotopes with 41-Mev and 48-Mev helium ions

	Isotope							
	Ni^{60}		Pd^{110}		Bi^{209}		U^{238}	
	41 Mev	48 Mev	41 Mev	48 Mev	41 Mev	48 Mev	41 Mev	48 Mev
Scattering-chamber cross section (mb)								
α,d	5.57	7.49	5.57	6.84	2.18	2.93	3.42	6.18
α,pn	81.4	76.3	30.5	28.9	15.8	15.7	10.8 6.16[a]	10.1 5.76[a]
α,d + α,pn	87.0±13.1	83.8±12.4	36.1±5.4	35.7±5.3	18.0±3.2	18.6±3.1	9.58±1.86[a]	11.9±2.4[a]
Radiochemically determined cross section (mb)								
	465±50	----	42.6±8.5	38.4±7.7	1.5[b]	----	6.8±1.0[b]	5.0±1.0[b]
$Q_{\alpha,pn} - Q_{\alpha,2n}$	8.6		6.6		4.6		5.1	

[a]Corrected for fission.

[b]Yield of long-lived isomer only.

the (α,pn) reaction obtained by radiochemical methods with those obtained from the scattering-chamber data.

The large maximum occurring in the (α,pn) excitation function for Ni^{60} cannot be accounted for by the direct mechanisms considered here. The (α,d) and (α,pn) cross sections obtained from scattering-chamber data remain approximately constant or increase as the helium-ion energy is increased from 40 to 48 Mev. The high-energy "tail" to the radiochemical cross sections is partly explained by the direct-interaction processes considered here. The (α,pn) reaction of Ni^{60} has been interpreted as proceeding by compound-nucleus formation and decay.[1] The large cross section for the evaporation of protons from the compound nucleus has been attributed to the low binding energy of protons relative to neutrons, and to possible large level-density differences between residual nuclei resulting from proton and neutron evaporation.[44,74] Similar conditions exist in the bombardments of Fe^{54} and Ni^{62}, as shown in Fig. 14.

Odd-odd nuclides have a greater level denisty and even-even nuclides a lesser density than odd-even nuclides. Weisskopf and Ewing have proposed that the even-even nuclides will in general have a level density 1/2 that of an even-odd and 1/4 that of an odd-odd nuclide.[75] However, experimental data obtained for nuclides in the region of nickel suggest that the difference in level density between even-even and odd-odd nuclides in this region may be as much as a factor of 10 or more.[42] As the probability of evaporation of a particle is directly proportional to the level density of the residual nucleus,[3] proton emission could be favored over neutron emission when proton emission leads to a much greater level denisty than neutron emission.

The observed maximum cross sections for the (α,pn) and (α,2n) reactions of Fe^{54}, Ni^{60}, and Ni^{62} occur at a helium-ion bombarding energy of about 32 Mev and are as follows:

Nuclide	$\sigma_{\alpha,pn}$ (mb)	$\sigma_{\alpha,2n}$ (mb)
Fe^{54}	500	10
Ni^{60}	950	250
Ni^{62}	475	Stable product formed.

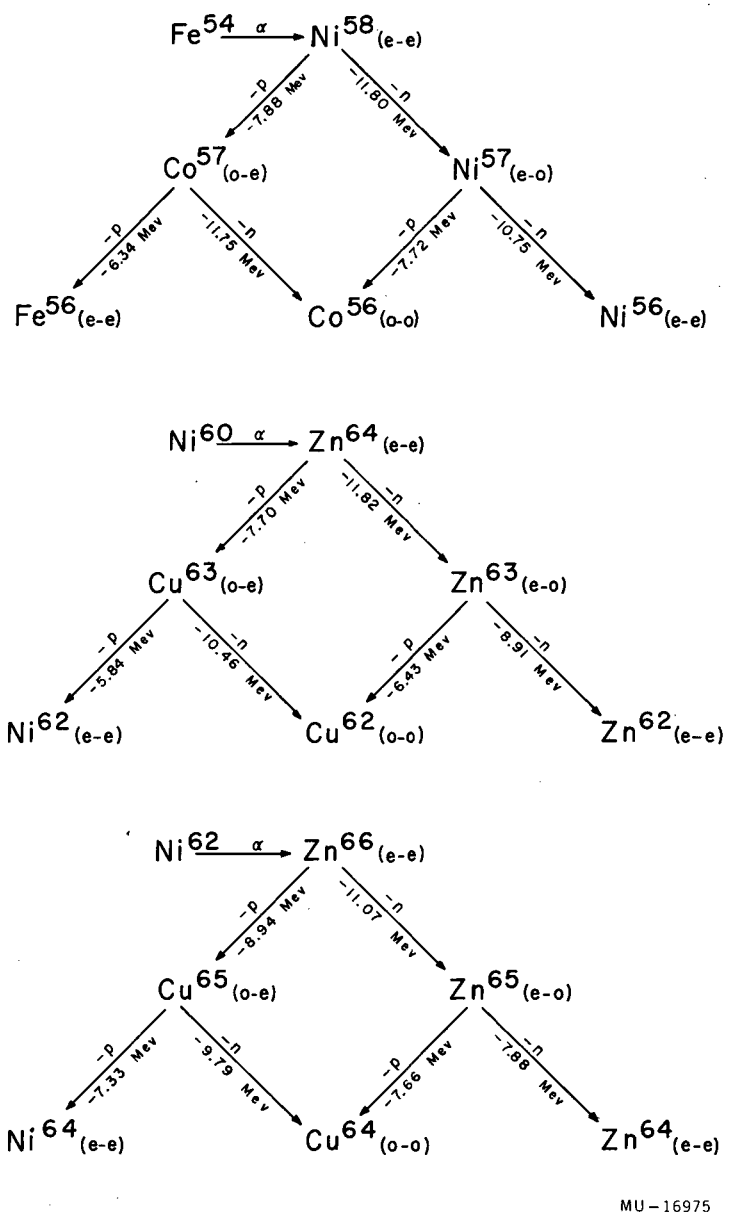

Fig. 14. Possible paths of evaporation of protons and neutrons from compound nuclei formed in the bombardment of Fe^{54}, Ni^{60}, and Ni^{62} with helium ions. Even-even (e-e), even-odd (e-o), odd-even (o-e), and odd-odd (o-o), refer to nuclear type. p and n refer to proton and neutron evaporation. The binding energies of protons and neutrons to the corresponding decaying nuclei are listed.

Because of the restrictions placed on the observable proton and deuteron energy ranges, and on the helium-ion bombarding energy, the present scattering-chamber data do not help much in showing whether the reaction proceeds by direct interaction or by way of a compound nucleus. For the present, the major part of the (α,pn) cross sections of Ni^{60}, Ni^{62}, and Fe^{54} appear to be best explained as proceeding by a compound-nucleus mechanism.

For the most part, the radiochemically determined (α,pn) cross sections obtained for nuclei heavier than nickel can be accounted for by the scattering-chamber data. The cross sections determined in the scattering chamber are larger than those determined radiochemically for Bi^{209} and U^{238} (the radiochemically determined data represent the yield of only the long-lived isomers); they are comparable to the 15 to 20-mb radiochemical cross sections of Pu^{238} and Th^{232}, however.

The magnitudes of the scattering-chamber cross sections exhibit a decrease with increasing Z as do the radiochemically determined cross sections. The decrease in the scattering chamber cross sections is due to three effects:

(a) A gradual decrease with Z in the total cross section for the production of protons and deuterons (about a 25 to 35% decrease in going from Pd^{110} to the heavy-element region, as estimated from the total energy spectra).

(b) A decrease in the fraction of the total energy spectra of the protons and deuterons associated with only the (α,d) and (α,pn) reactions, resulting in a lower cross section. This arises from the fact that the binding energy of a neutron to the product nucleus of the (α,d) and (α,pn) reaction decreases as Z increases, i.e., the energy ranges ($Q_{\alpha,d} - Q_{\alpha,dn}$) ($Q_{\alpha,pn} - Q_{\alpha,p2n}$) decrease with increasing Z. Table III shows that the binding energies changed by a factor of two in going from Ni^{60} to Bi^{209}.

(c) For the same excitation energy, the nuclear temperature decreases and the average evaporation energy of the neutron of the (α,pn) reaction decreases as the mass number increases. A decrease in the nuclear temperature, from about 2.0 Mev in Ni^{60} to less than 1 in U^{238}, decreased

the fraction of the total energy spectra of protons associated with only the (α,pn) reactions. A decrease in the nuclear temperature of 1 Mev decreases the (α,pn) cross section about 10%.

The (α,d) reaction constitutes only about 10 to 20% of the total scattering-chamber (α,pn) cross section in elements of lower Z than uranium. For elements in which fission may be induced in addition to spallation, the (α,d) reaction can become a larger fraction of the total cross section; the (α,d) reaction makes up about one-half the total (α,pn) cross section of U^{238}. The activation energies for fission are not very different from the neutron binding energies for many nuclei in which fission is induced.[76] The (α,d) direct interaction can leave residual nuclei excited to 4 to 6 Mev without inducing fission. The cross section for a process involving the prompt emission of a proton followed by neutron evaporation is reduced due to competition between neutron evaporation and fission. In this picture, the (α,d) reaction is an increasingly larger fraction of the total cross section as Γ_n/Γ_f for nuclei decreases.

The (α,d) reaction, as defined here, suffers little from fission competition. For the (α,pn) reaction, as defined here, there is fission competition at one step. For the (α,2n) reaction there is fission competition at two stages if both neutrons are evaporated. In addition, for nuclei of the same mass but differing in Z by one unit, Γ_n/Γ_f is from 2 to 10 times as large for the nuclide of the lower Z.[50] The total (α,pn) cross sections would not be expected to exhibit as large a reduction as the (α,2n) cross sections as one proceeds from nuclei in which fission is not induced to nuclei in which fission can be induced. The exact difference in reduction depends on the Γ_n/Γ_f of the nuclei involved, e.g., $U^{238} \sim 6$, $U^{233} \sim 30$ (assuming the direct-interaction contributions are the same for U^{233} as for U^{238}).

The broad maximum in the radiochemically determined excitation functions at a constant helium-ion energy of about 40 Mev for Pd^{110} and heavier elements are not explained by the scattering chamber data. More complicated processes than were considered here may be taking place.

F. Conclusions

It has been shown that, except for light elements in the region of nickel (possibly also elements of lower Z, as no radiochemical data were available), the (α,pn) reaction appears to proceed primarily by direct-interaction processes for incident helium ions of energy greater than 40 Mev. For the elements studied, the (α,d) reaction can account for less than half the (α,pn) "radiochemical" cross sections; a process involving proton and neutron emission is responsible for a large fraction of the reaction.

A simple mechanism, involving the prompt emission of a high-energy proton followed by neutron evaporation, permits calculation of (α,pn) cross sections from the measured proton spectra. When the calculated (α,pn) cross sections are combined with the (α,d) cross sections, their sum agrees fairly well with the radiochemical data for the elements heavier than nickel. This simple picture does not explain certain features of the radiochemical excitation functions, and a more complex process may be taking place: possible simultaneous emission of a medium-energy proton and neutron by a direct process.

Butler's theory gives a reasonably good fit to the angular distribution of the direct-interaction deuterons from the (α,d) reaction as well as the protons from the (α,p) reaction of Be^9.

ACKNOWLEDGMENTS

I wish to express my gratitude to Professor Glenn T. Seaborg for his support and encouragement during the performance of this work.

I would like to express my deep appreciation to Dr. Bernard G. Harvey for his help, guidance, and encouragement during the entire project.

I would also like to extend my appreciation to Dr. Jose Gonzalez-Vidal, Dr. William H. Wade, Dr. Homer Conzett, Dr. T. Darrah Thomas, and Dr. Norman Glendenning for many helpful discussions and ideas.

I am grateful to Dr. William H. Wade, George Merkel, Dennis Hoffman, and particularly Dr. Jose Gonzalez-Vidal for their help with the scattering-chamber techniques and acquisition of data.

I wish to thank Duane Mosier and Fred Vogelsberg for their advice and assistance in the operation and maintenance of the electronic equipment.

The cooperation of William Barclay Jones, Peter McWalters, John Wood, Robert Cox, and other members of the 60-inch cyclotron crew is greatly appreciated. Thanks are due Mrs. Patricia Howard for typing the final draft of this report.

Finally I would like to thank my wife, Joan, for help, understanding, and patience during the course of this work.

This work was performed under the auspices of the United States Atomic Energy Commission.

REFERENCES

1. S. N. Ghoshal, Phys. Rev. 80, 939 (1950).

2. N. Bohr, Nature 137, 344 (1936).

3. J. B. Blatt and V. F. Weisskopf, Theoretical Nuclear Physics, (John Wiley and Sons, New York, 1952).

4. Bruce M. Foreman, Spallation and Fission in Thorium-232 (Thesis), UCRL-8223, April 1958.

5. Vandenbosch, Thomas, Vandenbosch, Glass, and Seaborg, Phys. Rev. 111, 1358 (1958).

6. Glass, Carr, Cobble, and Seaborg, Phys. Rev. 104, 434 (1956).

7. S. T. Butler, Phys. Rev. 106, 272 (1957).

8. R. Serber, Phys. Rev. 72, 1114 (1947).

9. D. C. Peaslee, Ann. Rev. Nuclear Sci. 5, 99 (1955).

10. Eisberg, Igo, and Wegner, Phys. Rev. 100, 1309 (1955).

11. J. Gonzalez-Vidal, Survey of Tritium-Producing Nuclear Reactions (Thesis), UCRL-8330, June 1958; W. Wade and J. Gonzalez-Vidal, Spallation-Fission Competition in Heaviest Elements: Triton Production, UCRL-3640, March 1957.

12. F. N. Spiess, Phys. Rev. 94, 1292 (1954).

13. T. Sikkeland, S. Amiel, and S. Thompson, Spallation Reactions of Cf^{252} with Helium Ions, UCRL-8103, Jan. 1958.

14. Torbjørn Sikkeland (Lawrence Radiation Laboratory), private communication, Nov. 1958.

15. Jack Miller (Columbia Univ.), private communication to Bernard G. Harvey (UCRL), 1957.

16. Saadia Amiel (UCRL), unpublished data, 1957.

17. Susanne Ritsema, Fission and Spallation Excitation Functions of U^{238} (M.S. Thesis), UCRL-3266, Jan. 1956.

18. Aron, Hoffman, and Williams, U. S. Atomic Energy Commission Unclassified Document AECU-663, May 1951.

19. Bruce M. Foreman, Jr., unpublished data, 1955.

20. Robert Vandenbosch, Fission and Spallation Competition in Ra^{226}, Th^{230}, U^{235}, and Np^{237} (Thesis), UCRL-3858, July 1957.

21. D. L. Hufford and B. F. Scott, The Transuranium Elements: Research Papers, National Nuclear Energy Series, Vol. 14B, (McGraw-Hill Book Company, Inc., New York, 1949), p. 1149.

22. Separated Isotopes Division, Oak Ridge National Laboratory, Oak Ridge, Tenn.

23. W. Blum and G. Hogaboom, Principles of Electroplacting and Electroforming (McGraw-Hill Book Company, Inc., New York, 1949).

24. Organic Reagents for Metals (Hopkins and Williams, Ltd., London, England, 1938) p. 41.

25. Baker and Adamson, General Chemical Division, New York 6, N. Y.

26. A. D. Mackay Inc., 198 Broadway, New York, N. Y.

27. F. Spedding, Atomic Research Institute, Iowa State College, Ames, Iowa.

28. W. W. Meinke, Chemical Procedures Used in Bombardment Work at Berkeley, UCRL-432 (AECD-2738), Aug. 1949.

29. Donald Barr, Nuclear Reactions of Copper Induced by 5.7-Bev Protons (Thesis), UCRL-3793, May 1957.

30. W. Nervick and P. Stevenson, Nucleonics 10, 18 (1952).

31. Pacific Electro-Nuclear Company, Culver City, Calif. (Model PA-3).

32. M. Kalkstein and J. Hollander, A Survey of Counting Efficiencies for a 1-1/2-Inch-Diameter x 1-Inch-High Sodium Iodide (Thallium Activated) Crystal, UCRL-7764, Oct. 1954.

33. Strominger, Hollander, and Seaborg, Revs. Modern Phys. 30, 585 (1958).

34. W. L. Briscoe, Rev. Sci. Instr. 29, 401 (1958).

35. Robert E. Ellis, Elastic Scattering of 48-Mev Alpha Particles by Heavy Nuclei (Thesis), UCRL-3114, Aug. 1955.

36. Gerhard E. Fischer, The Scattering of 10-Mev Protons on Carbon and Magnesium (Thesis), UCRL-2546, May 1954.

37. Robert G. Summers-Gill, Some Properties of the Beryllium Nucleus Obtained from Scattering Data (Thesis), UCRL-3388, April 1956.

38. Robert E. Ellis, Robert G. Summers-Gill, and Franklin J. Vaughn, (UCRL), unpublished data, 1955.

39. Bichsel, Mozley, and Aron, Phys. Rev. 105, 1788 (1957).

40. M. Livingston and H. Bethe, Revs. Modern Phys. 9, 263 (1937).

41. Stokes, Northrup, and Boyer, Rev. Sci. Instr. 29, 61 (1958).

42. F. Ajzenberg and T. Lauristen, Revs. Modern Phys. 27, 77 (1955).

43. K. J. Le Couteur, Proc. Phys. Soc. (London) 63A, 259 (1950).

44. J. W. Meadows, Phys. Rev. 88, 143 (1952); ibid. 98, 744 (1955).

45. S. T. Butler and O. H. Hittmais, Nuclear Stripping Reactions (Wiley, New York, 1957).

46. J. Lang and K. Le Couteur, Proc. Phys. Soc. (London) 67A, 586 (1954).

47. G. Igo, Phys. Rev. 106, 256 (1957).

48. Geroge Merkel (UCRL), pricate communication, Dec. 1958.

49. Robert Vandenbosch (Argonne National Lab.), private communication to T. Darrah Thomas (UCRL), 1958.

50. R. Vandenbosch and J. Huizenga, Proceedings of the Second International Conference on Peaceful Usus of Atomic Energy, Geneva, 1958, (United Nations, New York, 1958), A/conf. 15/p/688.

51. J. Heidmann, Phys. Rev. 80, 171 (1950).

52. Cladis, Hess, and Moyer, Phys. Rev. 87, 425 (1952).

53. J. Wilcox, and B. Moyer, Phys. Rev. 99, 875 (1955).

54. A. Zucker, Proceedings of the Conference on Reactions Between Complex Nuclei (Gatlinberg, Tenn., May 1958) ORNL-2606.

55. G. E. Fischer, Phys. Rev. 96, 704 (1954).

56. Freemantle, Prowse, and Rotblat, Phys. Rev. 96, 1270 (1954); ibid. 96, 1270 (1954).

57. V. Weisskopf, Phys. Rev. 62, 295 (1937).

58. L. Wolfenstein, Phys. Rev. 82, 690 (1951).

59. W. Hauser and H. Feshback, Phys. Rev. 87, 366 (1952).

60. Dostrovsky, Rabinowitz, and Bivins, Phys. Rev. 111, 1659 (1958).

61. Eisberg, Igo, and Wegner, Phys. Rev. 93, 1039 (1954).

62. S. T. Butler, Proc. Roy. Soc. (London) A208, 559 (1951).

63. H. McManus and W. T. Sharp, Phys. Rev. 87, 188 *1952).

64. Austern, Butler, and McManus, Phys. Rev. 92, 350 (1953).

65. P. Von Herrmann and G. F. Pieper, Phys. Rev. 105, 1556 (1957); G. F. Pieper and N. P. Heydenburg, Phys. Rev. 111, 264 (1958).

66. C. E. Hunting and N. S. Wall, Phys. Rev. 108, 901L (1958).

67. S. T. Butler, Phys. Rev. 80, 1095 (1950).

68. S. T. Butler and E. E. Salpeter, Phys. Rev. 88, 133 (1952).

69. C. E. Hunting and N. S. Wall, Bull. Am. Phys. Soc. Ser. II 2, 181 (1957).

70. R. Sherr and M. Rickey, Bull. Am. Phys. Soc. Ser. II 2, 29 (1957).

71. A. P. French, Phys. Rev. 107, 1655 (1957).

72. Walter John, Jr., Systematics of Excitation Functions With Application to Lead (Thesis), UCRL-3093, Aug. 1955.

73. E. L. Kelley and E. Segrè, Phys. Rev. 75, 999 (1949).

74. Cohen, Newman, and Handley, Phys. Rev. 99, 723 (1955).

75. V. F. Weisskopf and D. H. Ewing, Phys. Rev. 57, 472 (1940).

76. Robert Vandenbosch and Glenn T. Seaborg, Phys. Rev. 110, 507 (1958).

This report was prepared as an account of Government sponsored work. Neither the United States, nor the Commission, nor any person acting on behalf of the Commission:

A. Makes any warranty or representation, expressed or implied, with respect to the accuracy, completeness, or usefulness of the information contained in this report, or that the use of any information, apparatus, method, or process disclosed in this report may not infringe privately owned rights; or

B. Assumes any liabilities with respect to the use of, or for damages resulting from the use of any information, apparatus, method, or process disclosed in this report.

As used in the above, "person acting on behalf of the Commission" includes any employee or contractor of the Commission, or employee of such contractor, to the extent that such employee or contractor of the Commission, or employee of such contractor prepares, disseminates, or provides access to, any information pursuant to his employment or contract with the Commission, or his employment with such contractor.